Dynamic carbon surface chemistry in electrolytic water oxidation

Yuxiao Ding,[1*] Qingqing Gu,[1] Alexander Klyushin,[2,3] Xing Huang,[2] Sakeb H. Choudhury,[1] Ioannis Spanos,[1] Feihong Song,[1] Pascal Düngen,[1] Anna K. Mechler,[1] Robert Schlögl[1,2] and Saskia Heumann[1*]

1. Max Planck Institute for Chemical Energy Conversion, Stiftstrasse 34-36, Mülheim an der Ruhr 45470, Germany

2. Fritz-Haber-Institut der Max-Planck Gesellschaft, Faradayweg 4-6, Berlin 14195, Germany

3. Research Group Catalysis for Energy, Helmholtz-Zentrum Berlin für Materialien und Energie GmbH

Albert-Einstein-Strasse 15, 12489 Berlin (Germany)

Email: Saskia.Heumann@cec.mpg.de, Yuxiao.Ding@cec.mpg.de

Carbon materials have been widely used as electrodes, but the mechanistic roles are still not clear due to the complexity of the carbon surface chemistry. Herein we clarify that intrinsic material properties of carbon have to be activated by extrinsic factors. Pure carbon has no catalytic activity when used as electrode for electrocatalytic water oxidation. The evolution of oxygen functional groups on the carbon surface with increasing potential and the subsequent formation of real active sites with iron impurities from the electrolyte have been confirmed. These in-situ formed active sites protect the carbon from deep oxidation. This unprecedented finding not only provides insight into the dynamic evolution of carbon electrode surface chemistry and raises awareness of the need for detailed surface analysis under operando conditions, but also suggests a direction for the development of scalable and high-performance carbon-based electrode systems for various electrochemical applications.

Carbon materials have been widely used as material solutions for sustainable use of energy from fuel cells via batteries, (photo)anodes and solar cells.[1] The excellent electron transfer ability of sp^2-hybridized carbon together with the ability to fine-tune its structures and properties are key points for advanced electrodes to meet the high demanding expectation. Considering the relatively low cost, environmental compatibility and sustainability, carbon materials could play key roles in future energy systems. However, due to the complexity of the carbon surface chemistry and the dynamic changes of the carbon surface during reactions, the understanding of the role of carbon in different applications is mainly driven by a trial-and-error approach. Determining the evolution of the carbon surface in different applications is essential for understanding the mechanism and design of appropriate knowledge-based electrodes. It is a big challenge to characterize the carbon surfaces in detail under real active conditions, since carbon materials hydrolyze in water and even more easily in alkaline or acidic electrolytes.[2] In addition, electrolytic water oxidation takes place at applied potentials, which can lead to deviations between the actual and measured structures if these are not carried out in-operando.

Electrolytic water splitting is of high relevance for the conversion of excessive renewable energy derived electricity into chemical energy and the most difficult elementary step is the anodic water oxidation part.[3] Carbon materials are used as low cost metal-free anode material for the anodic process.[4] However, carbon is not stable under the harsh oxidizing conditions[5] as carbon oxidation (0.207 V, NHE)[6] is much easier than water oxidation (1.23 V, NHE). This means when carbon is used for water oxidation, there must be different active sites other than carbon itself. Herein, we use highly graphitic carbon nanotubes (CNTs) as anode material for water oxidation, and by varying the surface properties of functional groups a good reaction rate can be reached. By the analysis of carbon surface oxygen functional groups, we illustrate the evolution of carbon surface chemistry during the reaction. Although carbon itself does not provide the direct active sites for water oxidation, phenol and carbonyl groups on the carbon surface are indispensable for the dynamic formation of the real active C-O-Fe site with the trace iron impurities of the electrolyte. A similar effect of activating intrinsic material properties by Fe impurities from the electrolyte is known for Ni-based catalysts.[7] Here, the formation of the active sites also prevents carbon from deep oxidation, therefore allowing carbon-based electrodes being used as water oxidation electrodes.

Results and Discussion

Viability of using carbon electrode for water oxidation and the dynamic surface chemistry

To determine whether carbon can perform well for water oxidation as an electrode, several carbon samples with different properties are compared under the same reaction conditions (details for all samples can be found in the Supporting Information, SI). Figure 1a shows the

electrochemical behavior of those samples in 0.1 mol/L KOH electrolyte. The original, as received CNTs contain some metal residues from the synthesis process, resulting in a medium water oxidation activity among all investigated samples. When the metal residues are removed by the treatment in nitric acid (100°C for 20 h, NA CNTs), the reactivity almost disappears for the obtained NA CNTs. Treatment of CNTs with mixed nitric and sulfuric acid (NSA CNT) introduces much more oxygen functional groups on the carbon surface,[8] which results in the highest activity in the measured cyclic voltammograms (CV) with an overpotential of 360 mV (for 10 mA/cm^2). In addition, as reference, a commercial $NiCoO_x$ sample shows an even higher overpotential (410 mV at 10 mA/cm^2) than the NSA CNTs under the same conditions, thus indicating a superior reactivity of the NSA CNTs. This is further confirmed by the key performance indicators (KPI) of the electrochemical data in Table S1. The detailed electrochemical performances and comparison with the tested carbon materials are also given in Figures S1-S7 and Table S2, revealing the viability of carbon as an anode material for water electrolysis.

Apparently, functional groups on CNTs do contribute to the activity. There are several different oxygen functional groups on carbon surfaces that lead to broad redox peaks in the cyclic voltammogram at around 0.5 VRHE (Figure S8). The low position of the oxidative peak confirms that the carbon oxidation is much easier than the water oxidation. Selective removal of specific functional groups can be achieved by varying the annealing temperature under Ar atmosphere (Figure S5).[9] This allows the direct assignment which functional groups contribute to the formation of active sites. For example, when carboxylic groups (CAR, black line) are removed by annealing at 253°C, the electrochemical performance in the linear sweep voltammogram (LSV) does not differ from the CNTs that contain all possible oxygen functional groups (NSA CNT, red line). This indicates that carboxylic groups do not contribute to the electrocatalytic activity. Applying this method to other temperatures/functional groups, the respective contribution to the electrocatalytic activity can be determined. From these results we conclude that carboxylic and anhydride groups do no contribute, while lactone, phenol and carbonyl groups are important for the activity. Considering that anhydride, ether and lactone groups will hydrolyze into carboxylic and phenol groups when they get in contact with the electrolyte, only carboxylic, phenol and carbonyl groups exist during the reaction.[2] All transformations of the functional groups are given in Figure S9. Accordingly, temperature-programmed desorption (TPD) of the CNTs soaked in the electrolyte exhibit only three main peaks, which are carboxylic, phenol and carbonyl groups, respectively (Figure 2c, S10 and S11). Based on the above results, it can be concluded that only phenol and carbonyl groups are involved in the formation of active sites. In Figure 2c, samples after different reaction times (20 min and 2 h) show similar amounts of functional groups compared to the original CNT

sample soaked in KOH. Only a slight change of the phenol and carbonyl group ratio can be observed.

To check whether the functional groups are formed in-situ during the oxidation process, O^{18} labeled water was used in the electrolyte. After 2h of electrocatalytic reaction, no O^{18} containing carbon oxides were detected (Figure S12), revealing that no new oxygen functional groups are formed on the surface during the reaction. This also confirms that the carbon surface does not show a continuous deep oxidation. For the sample annealed at 1000°C, where almost all functional groups are removed, there is still some current observable at higher potentials (Figure 2b, purple), and a slight increase can be observed in the chronoamperogram (CA) (Figure S13). This is because phenol groups on some dangling bonds and edge parts, produced during the annealing process can be formed in-situ by interaction with the hydroxide (Figure 2c, S14). Subsequently, the surfaces of the annealed CNTs are gradually functionalized again displaying a stable activity. Therefore, we can conclude that phenol groups, carbonyl groups and defects are useful for the reaction. Carbonyl groups and phenol groups are dynamically transferred via the keto-enol tautomerization into each other during the reaction (Figure 1c and 1d). These conclusions are in good accordance with our experimental investigations with model catalysts.[10]

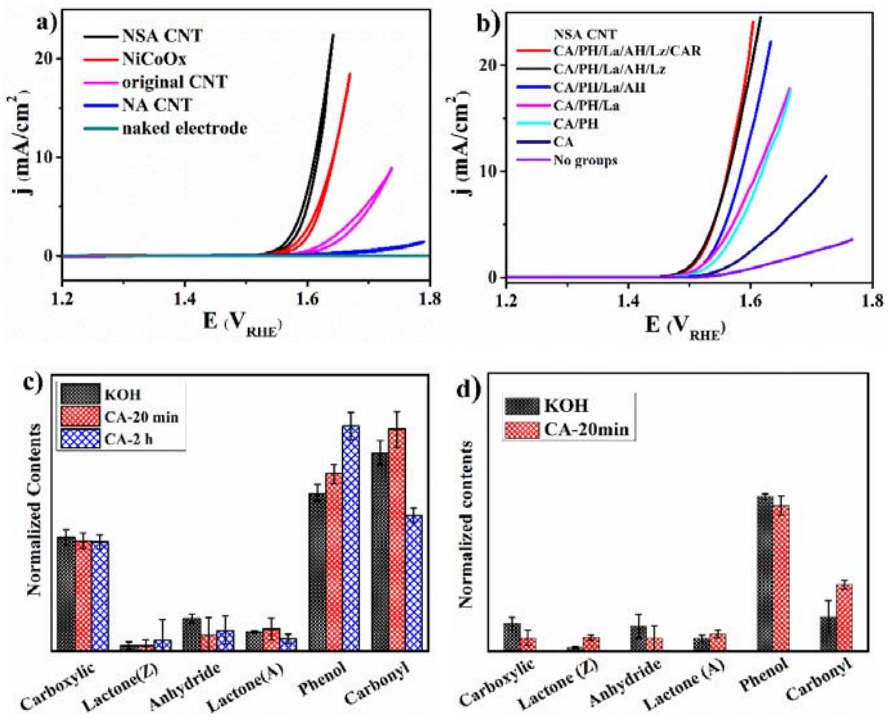

Figure 1. Influence of oxygen functional groups on the reaction and the evolution of different functional groups during the reaction. a) Cyclic voltammogram (CV) of the naked electrode, different CNTs and the commercial $NiCoO_x$ normalized to the geometric area of the active electrode area. b) Linear sweep voltammograms (LSV) of CNTs annealed at different temperatures, normalized to the geometric area of the active electrode area. Each annealing temperature results in the removal of one specific oxygen functional group. CAR = carboxylic group, Lz = lactone at zigzag position, AH = anhydrides, La = lactone at armchair position, PH = phenol/ether, CA = carbonyl group c) The content of the functional groups on soaked NSA CNT for 20 min in KOH (denoted as KOH), NSA CNT sample after 20 min CA (denoted as

CA-20min) and after 2 h CA test (denoted as CA-2h), respectively. d) The content of the functional groups of CNTs annealed at 1000°C and soaked in KOH (denoted as KOH) and the annealed sample after 20 min CA test (denoted as CA-20min). The amounts of the functional groups are obtained by TPD (Figure S10, S11 and S14). Considering the big error bars of the lactone and anhydride groups in Figure 2c and carboxylic, lactone and anhydride groups in figure 1d, the amount of these functional groups are neglectable.

The influence of amorphous parts on carbon and the carbon oxidation issue

Amorphous carbon is an unavoidable part of all carbon materials; therefore, it is necessary to clarify whether it influences the catalytic reactivity or not. In Figure 2a, the Raman spectrum of the sample soaked in 0.1 M KOH for 20 min (KOH) shows a decrease of the amorphous part in comparison to the NSA CNTs, which means the amorphous part exhibits physical detachment in the electrolyte. In addition, the color of the KOH solution becomes brownish after washing CNTs, while repeated washing of the same batch of CNTs in new solutions gradually makes the color of the solution transparent (Figure S15). This indicates that amorphous parts are removed away by this physical washing procedure. The electrolyte does not remove large graphitic layers. The brownish electrolyte was exposed to ultraviolet light, and yellow fluorescence could be observed, caused by carbon quantum dots from the amorphous parts (Figure S16).[11] Accordingly, the ultraviolet–visible spectrum of the brownish electrolyte in Figure S17 shows a peak at around 230 nm. The CNTs before and after the washing step show similar electrochemical behaviors (Figures S18, S19), suggesting that the amorphous part has no influence on the reaction. Transmission electron microscopy (TEM) images (Figure S20) and Near Edge X-Ray Adsorption Fine Structure (NEXAFS) C K-edge spectra (Figure 2b) of the CNTs before and after the electrochemical test confirmed the high stability of the graphitic backbone during the oxidation process. A more detailed view of the CNT surface by high-resolution TEM (HRTEM) is shown in Figure 2c. The amorphous carbon on the CNTs surface was mostly removed after 2 hours CA test. Raman spectrum of the sample after CA test shows similar peaks as compared to the other two samples (Figure 2a). From which one can conclude, when functionalized CNTs are used as anode, they show electrochemically stable behavior and undergo only physical detachment of amorphous carbon. A 92% Faraday efficiency of oxygen evolution can be obtained by testing the oxygen content (SI). Considering that not all oxygen can be detected by the oxygen sensor due to the bubble formation, the real efficiency should be close to 100%. Electrochemical carbon oxidation can be thus neglected for the CNT sample. Besides, the original oxygen on the carbon surface has no exchange with oxygen in the electrolyte, which is supported by the O^{18} labelled water experiment. Long-term stability tests (10 h at 1.8 VRHE in Figure S21) can also confirm that there is no obvious carbon oxidation of the functionalized carbon electrode. As mentioned above, carbon itself will be oxidized first instead of being the catalyst for water oxidation.

Therefore, there must be some newly formed active sites on the functional groups to protect carbon from deep oxidation.

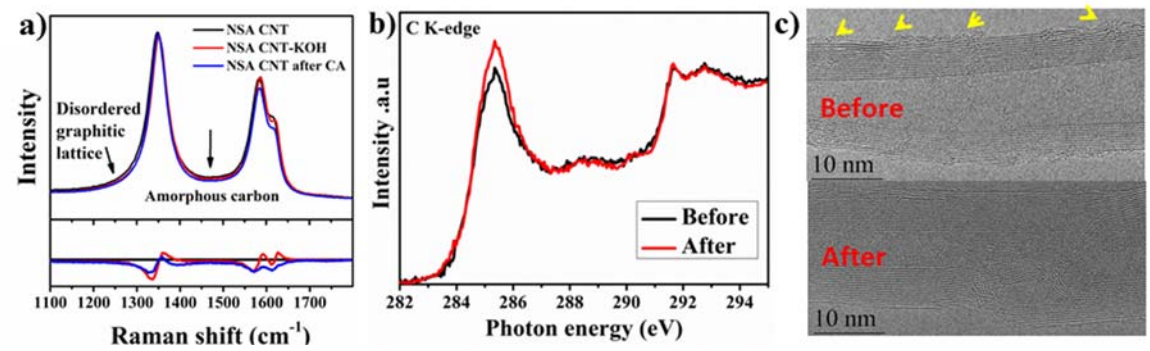

Figure 2. Carbon surface properties before and after reaction. a) Raman spectra of NSA CNT (black line), KOH soaked NSA CNT for 20 min sample (NSA CNT-KOH, red line), NSA CNT sample after 2 h CA test (NSA CNT after CA, blue line). The lower part is with the subtraction of the NSA CNT spectrum, from which a better view of the comparison can be observed. b) NEXAFS spectra of the C K-edge of the CNTs before and after reaction. c) HRTEM images of the NSA CNT before and after 2 hours CA measurement.

The real active site for water oxidation

Oxygen functional groups on carbon surfaces play a large role in the activity, but cannot be the actual active sites. The reactivity of NSA CNTs significantly decreased to a very low level (Figure 3a) when iron purified electrolyte was used (reduced iron content from 4 ppb to near 0 ppb, SI).[12] In addition, the low activity decreases further over time, which can be attributed to carbon oxidation, as the protection of the real active sites by Fe-species is lacking (Figure S22). This suggests that the high activity of water oxidation needs the presence of both components, functional groups and iron impurities. The in-situ formed C–O–Fe species are therefore very likely the real catalytic sites (Figure S23, S24). NEXAFS spectra of the Fe L-edge before and after the CA test provide a direct evidence for the in-situ trapping of iron species on CNTs during the electrocatalytic reaction (Figure 3b). The Fe 2p spectrum measured with synchrotron X-ray photoelectron spectroscopy (XPS) also supports the existence of the iron on CNTs after the electrochemical reaction (Figure S25).

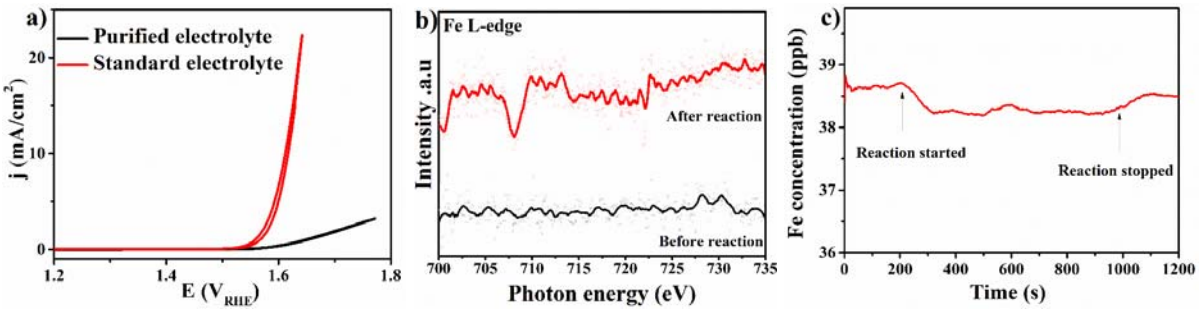

Figure 3. Confirmation of the dynamic formation of the active sites. a) CV measurements of NSA CNTs in standard and purified electrolyte. b) (NEXAFS) spectra of the CNT sample Fe L-edge before and after CA test. c) In-situ ICP-OES measurement of iron concentration in the flowed electrolyte through the reaction (details in SI).

Furthermore, systematically varied iron contents in the electrolyte show a remarkable influence on the activity (Figure 4a), evidencing the dynamic formation of active sites by bonding the functional groups with iron. All these information confirm the in-situ formation of catalytically active C–O–Fe sites during the reaction. In alkaline media, the iron species most likely exist as Fe^{3+}. Therefore, based on the experimental evidences, a C–O–$Fe(OH)_2$ species is proposed as the reactive sites for OER (Figure S26). The in-situ formation of the active sites with a continuous adsorption of the iron cations can be directly observed by the reduced Fe concentration detected by online inductively coupled plasma-optical emission spectroscopy (ICP-OES) in a flow-cell system (Figures 3c, S27). Time-dependent observations reveal an eight-minute initial activation step to reach a stable current, pointing to the dynamic formation of the active species at high potentials (Figure 4b). Applied differential pulse voltammetry measurements (DPV) show a much higher iron oxidation peak after the CA test which can be explained by a higher Fe-concentration of dynamically formed C-O-Fe species during the OER (Figure 4c). Several molecular iron-based water oxidation catalysts have been developed.[13] Typically, their activity is lower than the current system and we also checked several other iron-based systems under the same conditions, which show much lower activity (Figure S28). These also confirm the iron species here is not only to prevent deep electrode oxidation, but also useful for fabricating efficient water splitting devices. It is promising to substitute the iron with other metals, which will be conducted in our following work.

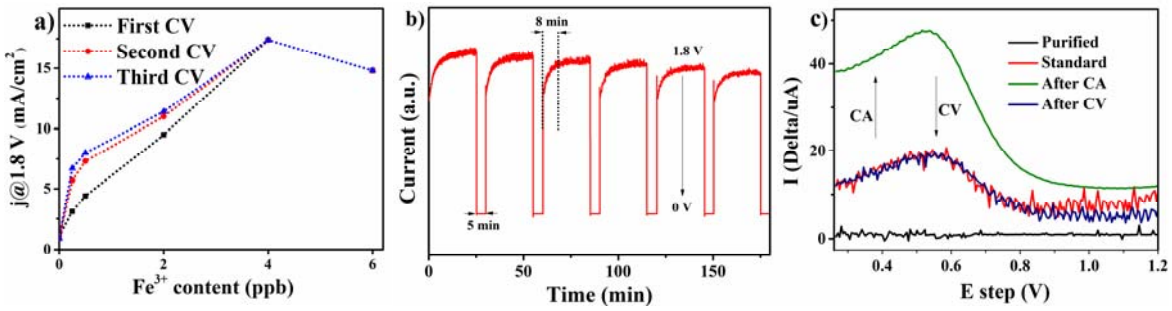

Figure 4. a) The current of the functionalized CNT at 1.8 V in the electrolyte with different iron contents. The measurement is conducted independently for each iron content. b) On and off CA measurements between 1.8 V and 0 V. The test was performed with standard 0.1 M KOH. c) DPV measurement of the sample is conducted before reaction, after CA, and after CV (all tests are done in one batch). The peak represents the iron content to some content. (details in the last part of SI).

All above in-situ measurements indicate that the formation of iron active sites is a dynamic process that takes place preferentially at high potentials. A possible mechanism is thus proposed showing the production of O_2 by C–O–Fe species (Figure S29). In general, it is proposed that the loss of the first electron couples with the reaction between Fe–OH and a hydroxyl ion produce a H_2O molecule. Subsequently, a formed radical could adsorb another hydroxyl ion to generate a FeOOH structure, while losing a second electron in this process. The loss of the third electron could be combined with a H_2O formation. In the last step, a FeOO–OH intermediate could be formed, which loses an electron during the formation of O_2.

Conclusion

Pure carbon cannot be a catalytic material for the electrocatalytic water oxidation, as it will be oxidized before catalyzing water oxidation. For the first time, we disclosed the dynamic change of the carbon surface chemistry during water splitting process and confirmed that specific oxygen functional groups on carbon surface play important role for the water oxidation. These functional groups can in-situ react with iron impurity in the electrolyte forming C-O-Fe as intrinsic active sites for the reaction, which also protects the carbon surface from deep oxidation. Although carbon itself can be oxidized at oxidative potential, the special combination of functional groups and iron makes carbon-based materials a suitable anode material for water electrolysis. Due to the diversity of carbon materials, the system can be potentially used as scalable and sustainable anode solution for water splitting and also gets a chance to be applied in broad material synthesis, catalysis and electrocatalysis. Different metal species could possibly work even better for the system.

Keywords: carbon chemistry • carbon catalysis • carbon electrode • water splitting • iron impurity

Experimental Section

The electrochemical measurements were conducted in a three-electrode system, which was controlled by using a potentiostat/galvanostat (BioLogic VSP, France). A platinized Pt wire as a counter electrode and a reversible hydrogen electrode (RHE, HydroFlex, Gaskatel GmbH) as a reference electrode. The XPS and NEXAFS experiments were performed at the ISISS beamline at the synchrotron radiation facility BESSY II of the Helmholtz Zentrum Berlin. The measurements were carried out in a stainless steel NAP-XPS chamber. The powder samples were pressed into a pellet of 8 mm diameter. Samples were placed between a stainless steel backplate and lid (with 6 mm hole) and mounted onto a sapphire sample holder. The NEXAFS spectra were obtained by recording the total electron yield (TEY). TPD was performed using a STA 449 F3 Jupiter® QMS4 setup from Netzsch with an argon gas flow of 50 ml/min. Raman spectra were measured by a Thermo Scientific DXR Raman Microscope with a 50x magnification and a 532 nm laser. TEM and HRTEM images were recorded with a double Cs-corrected JEOL ARM 200 transmission electron microscope with a cold field emission gun. The instrument was operated at 200kV.

Acknowledgements

The authors thank for support of the Max Planck society. The authors are grateful to N. Kowalew and Teresa Stamm (MPI-CEC) for assistance with carbon treatment, and B. Deckers (MPI-CEC) for assistance of graphic improvement. D. Shin, and S. Ye (MPI-CEC) are also thanked for fruitful discussions.

Author contributions

Y.D. conceived the research, carried out material treatment and basic characterization and performed the electrocatalytic tests. Q.G. carried out part of the sample treatment and electrocatalytic tests. A.K. performed and analyzed the NEAFS and XPS. X. H. contributed the TEM characterizations. S.C. contributed the Raman characterizations. I.S. contributed the operando ICP-OES study F.S. contributed the DPV characterization. P.D. contributed TPD part. R.S. and S.H. supervised the whole project. Y.D. wrote the manuscript with input from R.S. and S.H. All authors contributed to data analysis and manuscript revision.

Competing interests

The authors declare no competing interests.

References

[1] a) D. S. Su, S. Perathoner, G. Centi, *Chem. Rev.* **2013**, *113*, 5782-5816; b) Q. Zhang, X. B. Cheng, J. Q. Huang, H. J. Peng, F. Wei, *New Carbon Mater.* **2014**, *29*, 241-264; c) J. Briscoe, A. Marinovic, M. Sevilla, S. Dunn, M. Titirici, *Angew. Chem. Int. Ed.* **2015**, *54*, 4463-4468; d) T. Q. Lin, I. W. Chen, F. X. Liu, C. Y. Yang, H. Bi, F. F. Xu, F. Q. Huang, *Science* **2015**, *350*, 1508-1513; e) L. J. Yang, J. L. Shui, L. Du, Y. Y. Shao, J. Liu, L. M. Dai, Z. Hu, *Adv. Mater.* **2019**, *31,*1804799-1804799.

[2] S. Reiche, R. Blume, X. C. Zhao, D. S. Su, E. Kunkes, M. Behrens, R. Schlögl, *Carbon* **2014**, *77*, 175-183.

[3] a) N. S. Lewis, D. G. Nocera, *Proc. Natl. Acad. Sci. U. S. A.* **2006**, *103*, 15729-15735; b) R. Eisenberg, H. B. Gray, *Inorg. Chem.* **2008**, *47*, 1697-1699; c) M. G. Walter, E. L. Warren, J. R. McKone, S. W. Boettcher, Q. X. Mi, E. A. Santori, N. S. Lewis, *Chem. Rev.* **2010**, *110*, 6446-6473.

[4] a) X. Y. Lu, W. L. Yim, B. H. R. Suryanto, C. Zhao, *J. Am. Chem. Soc.* **2015**, *137*, 2901-2907; b) A. M. El-Sawy, I. M. Mosa, D. Su, C. J. Guild, S. Khalid, R. Joesten, J. F. Rusling, S. L. Suib, *Adv. Energy Mater.* **2016**, *6*; c) Y. Zhang, X. L. Fan, J. H. Jian, D. S. Yu, Z. S. Zhang, L. M. Dai, *Energy Environ. Sci.* **2017**, *10*, 2312-2317.

[5] C. Spori, J. T. H. Kwan, A. Bonakdarpour, D. P. Wilkinson, P. Strasser, *Angew. Chem. Int. Ed.* **2017**, *56*, 5994-6021.

[6] Kinoshita, K. in *Carbon: Electrochemical and Physicochemical Proper-ties*, *Vol. 3-12*. United States: N. p., **1988**. Web.

[7] J. Wang, L. Gan, W. Zhang, Y. Peng, H. Yu, Q. Yan, X. Xia, X. Wang, *Sci. Adv.* **2018**, *4*, 7970.

[8] P. Düngen, M. Prenzel, C. Van Stappen, N. Pfänder, S. Heumann, R. Schlögl, *Mater. Sci. Appl.* **2017**, *8*, 628-641.

[9] P. Düngen, R. Schlögl, S. Heumann, *Carbon* **2018**, *130*, 614-622.

[10] a) Y. M. Lin, K. H. Wu, Q. Lu, Q. Q. Gu, L. Y. Zhang, B. S. Zhang, D. S. Su, M. Plodinec, R. Schlögl, S. Heumann, *J. Am. Chem. Soc.* **2018**, *140*, 14717-14724; b) Y. Lin, Q. Lu, F. Song, L. Yu, A. K. Mechler, R. Schlögl, S. Heumann, *Angew. Chem. Int. Ed.* **2019**,8917-8921.

[11] H. T. Li, X. D. He, Z. H. Kang, H. Huang, Y. Liu, J. L. Liu, S. Y. Lian, C. H. A. Tsang, X. B. Yang, S. T. Lee, *Angew. Chem. Int. Ed.* **2010**, *49*, 4430-4434.

[12] I. Spanos, M. F. Tesch, M. Yu, H. Tüysüz, J. Zhang, X. Feng, K. Müllen, R. Schlögl, A. K. Mechler, *ACS Catal.* **2019**, 9, 8165-8170.

[13] a) W. C. Ellis, N. D. McDaniel, S. Bernhard, T. J. Collins, *J. Am. Chem. Soc.* **2010**, *132*, 10990-10991; b) J. L. Fillol, Z. Codola, I. Garcia-Bosch, L. Gomez, J. J. Pla, M. Costas, *Nature Chem.* **2011**, *3*, 807-813; c) K. G. Kottrup, D. G. H. Hetterscheid, *Chem. Commun.* **2016**, *52*, 2643-2646.

Supporting Information

Dynamic carbon surface chemistry in electrolytic water oxidation

Yuxiao Ding,*[a] Qingqing Gu,[a] Alexander Klyushin,[b,c] Xing Huang,[b] Sakeb H. Choudhury,[a] Ioannis Spanos,[a] Feihong Song,[a] Pascal Düngen,[a] Anna K. Mechler,[a] Robert Schlögl,[a,b] and Saskia Heumann*[a]

[a] Max Planck Institute for Chemical Energy Conversion, Stiftstrasse 34-36, Mülheim an der Ruhr 45470, Germany

[b] Fritz-Haber-Institut der Max-Planck Gesellschaft, Faradayweg 4-6, Berlin 14195, Germany

[c] Research Group Catalysis for Energy, Helmholtz-Zentrum Berlin für Materialien und Energie GmbH, Albert-Einstein-Strasse 15, Berlin 12489, Germany

Email: Saskia.Heumann@cec.mpg.de; Yuxiao.Ding@cec.mpg.de

Materials

Original CNT

Original CNT produced by Shandong Dazhan Nano Materials Co. is multi-walled CNT with average diameter around 10 nm and a BET surface area of 267 m²/g. The residues of the metal impurity of the samples are determined by total reflection x-ray fluorescence (TXRF). For the original CNT, the iron content is determined as 0.59wt%.

NA CNT

NA CNT is the original CNT washed with nitric acid. The washing step is: 20 g of MWCNT were mixed with 1000 ml of acid (68%), stirred and heated up under reflux at around 100 °C for 20 h. After the reaction the gaseous supernatant was purged with nitrogen to remove acidic vapor for better handling. The material was filtered and washed extensively in a washing cell over night with distilled water to remove residual acid and impurities like iron. After that, the black wet CNT was dried in drying oven at 100 °C for 20 h. The as-obtained CNT powder is NA CNT. The residues of the metal impurity of the samples are determined by total reflection x-ray fluorescence (TXRF). After washed by nitric acid, the iron content of NA CNT decreases to 0.19wt%.

NSA CNT

The pristine CNT was treated with mixed nitric and sulfuric acid (NSA, 65% nitric acid and 98% sulfuric acid; Vol% ratio of two acids is 1:1) to generate oxygen containing functional groups on the CNT surface. In a typical procedure, 10 g pristine CNT was mixed with 500 ml acid at 105 °C and stirred for 4 hours. Resulting nitrous gases were neutralized with 3 mol/L NaOH solution. Afterwards, the oxidized CNT were filtered. The residuals of the acid and catalyst were washed out over for several hours with flow cell. The CNT then was dried in a drying oven at 100 °C for 20 h. The as-obtained CNT powder is NSA CNT. The iron content was confirmed by TXRF as 0.05wt%, which is the lowest one during all the samples.

Experimental details

Pretreatment of electrodes

Working electrode is 5 mm Ø glassy carbon (GC) disk electrode in PEEK sheath. Proper electrode pretreatment to get a mirror-like surface is done before every measurement. Before the first use, electrodes are sandpapered with decreasing roughness. Electrodes are polished with polishing paste (Al_2O_3 slurry; 1.0 µm and 0.05 µm) on a wet polishing cloth for 3-5 minutes, and rinsed thoroughly with water. No scratches are visible on the glassy carbon surface. Before drop-coating of catalyst, electrodes are ultrasonicated in absolute ethanol for 5 minutes, rinsed thoroughly with water, ultrasonicated in millipore water for 5 minutes, rinsed thoroughly with water and dry in oven at 60 °C.

Ink preparation

Ink consists of 4 mL IPA, 960 µL H_2O and 40 µL Nafion solution (binder) and 5 mg sample. The catalyst is dispersed in the solvent by 15 min of ultrasonication. Proper dispersion yields a well dispersion without obvious particles. The catalyst precipitates from the dispersion over time. If any black precipitate can be seen, ultrasonication is repeated. The ink is used as soon as possible after been taken out from the ultrasonic bath.

Dropcoating

Electrodes with 50µg/cm² loading were produced. Volumes of 5 µL (twice) are pipetted onto the pretreated GC electrodes at room temperature and dried for 0.5 hours at 60 °C with a light uniform film formed on the electrode surface.

Electrolyte

KOH buffer solution is bought from Honeywell Research Chemicals. The buffer solution then was dissolve with ultrapure water to form 0.1 M KOH solution. The iron content in the standard solution was detected by ICP-OES to be 4 ppb, which is a very low level. Further purification was conducted by electrochemical deposition method using a special Ni-Co oxide catalysts, details can be found here (Ioannis Spanos, Marc F. Tesch, Mingquan Yu, Harun Tüysüz, Jian Zhang, Xinliang Feng, Klaus Müllen, Robert Schlögl, and Anna K. Mechler, ***ACS Catal.***2019, 9, 8165-8170*)*

The iron content is also confirmed by ICP-OES to be close to 0 ppb. Additional impurities of other metal species could not be detected by ICP-OES.

Electrochemical procedure

Electrochemical measurements comprise conditioning of work electrode, measurement of the open circuit potential (OCP), impedance spectroscopy (determination of iR-drop), cyclic voltammetry (CV, “activity”) and constant-potential chronamperometry (CA, “stability”). All the procedures are done in 0.1 M KOH.

Conditioning

This part of the procedure consists of the determination of the open circuit potential (OCP) for 60 s and a subsequent linear sweep from the OCP to 1 V_{RHE} (5 mV/s) to avoid a harsh potential jump and stress on the working electrode. Conditioning is done by 30 cycles at 100 mV/s from 0 V_{RHE} to 1 V_{RHE}.

Impedance spectroscopy (determination of iR-drop)

The uncompensated resistance (Ru, iR-drop) of the system is determined by electrochemical impedance spectroscopy (EIS) at the OCP. The first step is the determination of the OCP (for 60 s). EIS is carried out at the OCP: 25 data points between 100 kHz and 10 Hz with an amplitude of 10 mV_{RMS}. Ru is obtained using the resistance at 100 kHZ.

Cyclic voltammetry (“activity measurement”)

The cell remains switched on after EIS and the potential is swept from the OCP to 1 V_{RHE} (5 mV/s). Before start of the CV, the electrode is set to rotate at 1600 rpm. Cyclic voltammetry is conducted from 1 V_{RHE} to 1.8 V_{RHE} at 5 mV/s with automatic iR-compensation using Ru from impedance spectroscopy.

Chronoamperometry (CA)

To perform a stability test in chronoamperometric mode, the potential is kept at 1.8 V after stationary polarization for two hours or ten hours.

Temperature programmed desorption (TPD)

Thermal analysis was performed using a STA 449 F3 Jupiter® QMS4 setup from Netzsch with an argon gas flow of 70 ml/min. Isothermal steps were inserted during thermogravimetric mass spectroscopy analysis to separate functional groups with different decomposition temperatures. The optimum temperature of the implemented isothermal step was judged by the peak shapes of CO_2^+ signal. Based on the investigated results a heating rate of 20 K/min was applied in-between the isothermal steps to avoid overheating while maintaining satisfactory signal intensities, whereas a heating rate of 50 K/min was chosen after the last isothermal step, due to higher signal intensities.

Oxygen quantification

All measurements were conducted in 0.1M KOH, with internal resistance (IR)-correction. A coil-shaped platinized platinum wire (PT-5W, 125µm diameter, 99.99%, Science Products GmbH), placed along the flow channel following the electrolyte flow, was used as the counter electrode (CE), while the reference electrodes (RE) (Hg/HgO, CH Instruments Inc., CHI152, reference potential +0,098Vvs NHE) was inserted perpendicular to the electrolyte outlet channel. All potentials are expressed vs the RHE potential scale. Catalysts were drop casted on glassy carbon support measuring a surface area of 0.196 cm^2, previously polished with fine 0.05µm and 1.0µm alumina powder and ultra-sonicated for 15 min in MilliQ water. Catalyst inks were prepared by mixing and ultra-sonicating 49% H_2O, 49% ethanol and 2% Nafion solution for 30 min. Subsequently, a certain amount of catalyst ink was drop casted on the glassy carbon working electrode (WE) until a loading of 50 µg/cm^2 was achieved. The catalyst ink was dried on the glassy carbon support under an argon stream for 30 min and finally the working electrode sample holder was inserted into the flow cell. For all electrochemical characterizations, a flow rate of 0.86 ml/min was used, because it provides a good balance between oxygen gas removal from the catalyst surface.

Differential pulse voltammetry measurements (DPV)

The differential pulse technique discriminate faradic current from capacitive one. In this technique, the applied potential wave is the summation of a pulse train and a staircase from the initial potential to the final potential, and the current is sampled just before the pulse and close the end of the pulse. The final current recorded is the difference between these two

currents. The detailed experimental parameters are listed here: pulse hight (PH), step height (SH), pulse width (PW) and step time (ST) are 45 mV, 5 mV, 100 ms and 500 ms, respectively.

Table S1. The key performance indicators (KPI) of electrochemistry data of the NSA CNT and $NiCoO_x$.

Name	µg catalyst	Geometric area	Electrolyte, PH	Protocol
NSA CNT	10	0.19625 cm^{-2}	0.1 M KOH, 13	
OCP	Ru		Initial EIS measurement	
1.15 V_{RHE}	35.6 Ω			
E_{2mA/cm^2}	E_{5mA/cm^2}	E_{10mA/cm^2}	Initial activity measurement	
1.58 V_{RHE} (auto iR-drop)	1.60 V_{RHE} (auto iR-drop)	1.62 V_{RHE} (auto iR-drop)		
$J_{m,1.6V}$	$J_{m,1.7V}$	$J_{m,1.8V}$	Mass activity in mA/µg	
0.041	0.21	0.41		
J t=0 h	J t=0.5 h	J t=2 h	Stability at 1.8 V_{RHE}	
18.8 mA/cm^2	23.1 mA/cm^2	23.6 mA/cm^2		
Name	**µg catalyst**	**Geometric area**	**Electrolyte, PH**	**Protocol**
$NiCoO_x$	10	0.19625 cm^{-2}	0.1 M KOH, 13	
OCP	Ru		Initial EIS measurement	
1.03 V_{RHE}	35.4 Ω			
E_{2mA/cm^2}	E_{5mA/cm^2}	E_{10mA/cm^2}	Initial activity measurement	
1.55 V_{RHE} (auto iR-drop)	1.62 V_{RHE} (auto iR-drop)	1.64 V_{RHE} (auto iR-drop)		
$J_{m,1.6V}$	$J_{m,1.7V}$	$J_{m,1.8V}$	Mass activity in mA/µg	
0.028	0.17	0.36		
J t=0 h	J t=0.5 h	J t=2 h	Stability at 1.8 V_{RHE}	
15.0 mA/cm^2	19.2 mA/cm^2	18.6 mA/cm^2		

It is known that transition-metal oxides have high resistance. The resistance of NSA CNT, NA CNT and $NiCoO_x$ at 10 Hz are 65.5, 165.8 and 344.5 Ω, respectively. $NiCoO_x$ shows a higher

resistance due to the intrinsically insufficient electrical conductivity. The NSA CNT has more oxygen functional groups on the surface, but shows a lower resistance than the NA CNT. The reason might be the functional groups that make the CNT more hydrophilic, so the mass transfer between the carbon surface and the electrolyte are easier than the relatively more hydrophobic NA CNT. This also indicates that the formation of functional groups has no negative influence on the charge transfer process.

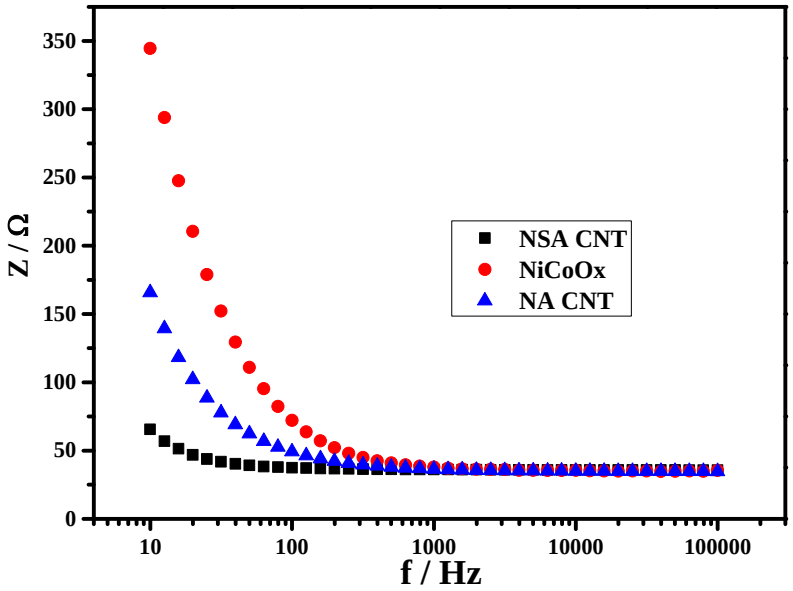

Figure S1. EIS at the open circuit potential (OCP) of different samples. The first step is to determine the OCP. EIS is carried out at the OCP: 25 data points between 100 kHz and 10 Hz with an amplitude of 10 mV.

As shown in Figure S2, a Tafel slope of 44.5 mV/decade was obtained for the NSA CNT, which is lower than $NiCoO_x$ in the reaction (48.2 mV/decade). This is also comparable with reported

metal-containing samples in literatures (Figure S3). NA CNT shows a Tafel slope of 225.4 mV/decade. From Raman analysis (Figure S4), NA CNT has more graphitic percentage than the NSA CNT sample. As we mentioned in the main text, graphitic structure has no obvious contribution to the reaction. Therefore, the oxygen functional groups might be the main contribution for OER. Since the detailed reaction mechanism is not clear, only a mathematic explanation is given on the obtained Tafel slopes. For the NSA CNT sample, that is, every 10 mA increase of the current needs 44.5 mV increase of the potential; while for the NA CNT every 10 mA increase of the current need 225.4 mV increase of the potential. Apparently, the lower the slope is, the better performance it has, as the lower potential means the lower energy it need to get the same amount of the products. Figure S3 and Table S2 show some comparison of the highly active transition-metal and carbon-based catalysts for OER. The current dynamic anode system is the first time to consider the application of the electrolyte. From the comparison, we can see that, with only the ppb level iron impurity, the functionalized CNT shows better performance than other samples, which means the trapping of the iron impurity with carbon is very promising.

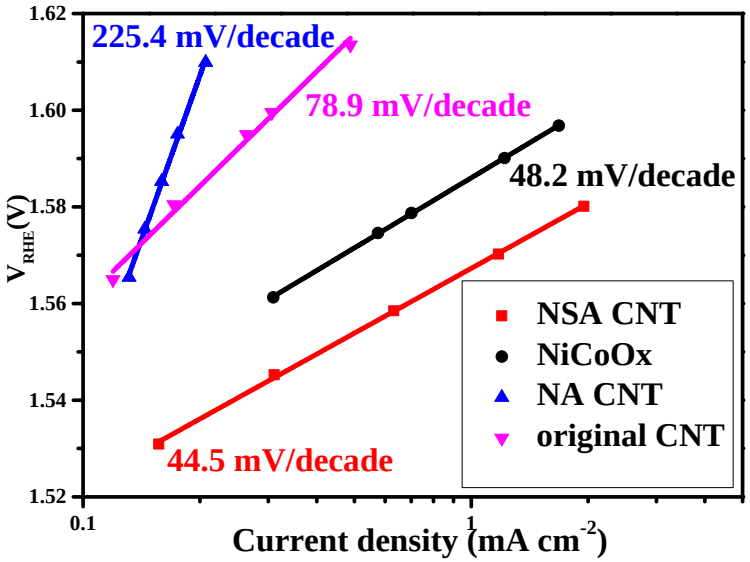

Figure S2. Tafel plots of different samples in Figure 1a.

Accurately comparing the intrinsic activity of different materials is very challenging. Here, the list of results from different materials is just a review of different results. As the conditions

used are totally different, the comparison is just a rough comparison to show that the NSA CNT is also a good anode material. The purpose of the current work is not to find the best material, but to find the mechanism of the carbon in the high oxidation potential and explain why carbon is not oxidized into carbon dioxide.

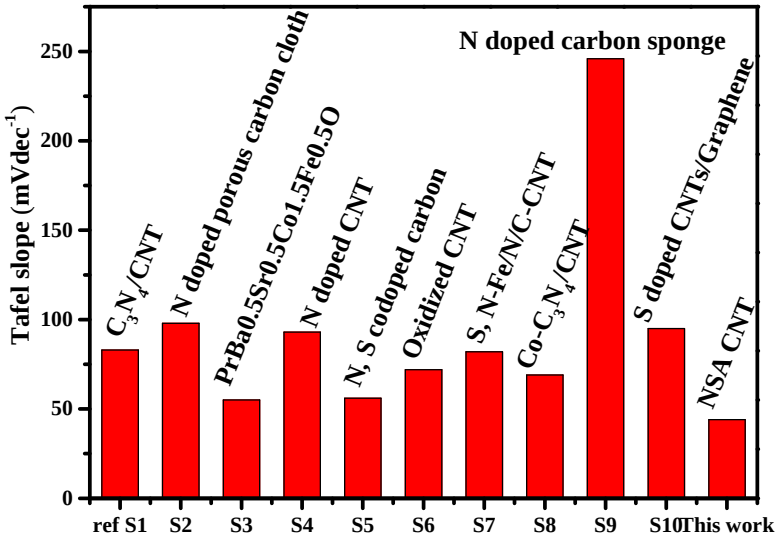

Figure S3. Comparison with the reported carbon-related OER catalysts. The detailed information for these references is provided in Table S2.

Table S2. Comparison of the highly active transition-metal and carbon-based catalysts for OER.

Reported Catalysts	η(mV) @10mA/cm^2	Electrolyte	Tafel slope (mVdec^{-1})	Literature
Ref S1. C_3N_4/CNT	370	0.1M KOH	83	**Angew. Chem. Int. Ed**., *2014*, 53, 7281 –7285
Ref S2. N-doped porous carbon cloth	360	1M KOH	98	**Energy Environ. Sci**., *2016*, 9, 3411--3416
Ref S3. $PrBa_{0.5}Sr_{0.5}Co_{1.5}Fe_{0.5}O_{\delta}$	358	0.1M KOH	55	**Nat. Commun**., *2017*, 8, 14586.
Ref S4. N-doped CNTs	370	0.1 M KOH	93	**Nat. Energy**, *2016*, 1, 15006.
Ref S5. N,S-codoped carbon materials	360	1M KOH	56	**Adv. Energy Mater**., *2017*, 1602068
Ref S6. Oxidized CNTs	450	0.1 M KOH	72	**J. Am. Chem. Soc**., *2015*, 137, 2901–2907
Ref S7. S,N-Fe/N/C-CNT	370	0.1 M KOH	82	**Angew. Chem. Int. Ed**., *2017*, 56,: 610-614.
Ref S8. Co-C_3N_4/CNT	380	1 M KOH	69	**J. Am. Chem. Soc**., *2017*, 139, 3336–3339
Ref S9. N-doped carbon microtube sponge	290	0.1 M KOH	246	**Energy Environ. Sci**., *2016*, 9, 3079-3084
Ref S10. S-doped CNTs/Graphene Nanolobes	350	1 M KOH	95	**Adv. Energy Mater**., *2016*, 6, 1501966

A fitting procedure based on single-phonon resonances for the Raman spectra of the CNT samples has provided us the opportunity to gain detailed and statistically significant information regarding the D- , G- , and D'-bands of samples with relatively high quantities of graphitic structures. As can be seen in Figure S4, the total defects and graphitic part ratio D*/G shows a trend of NSA CNT > NA CNT > original CNT.

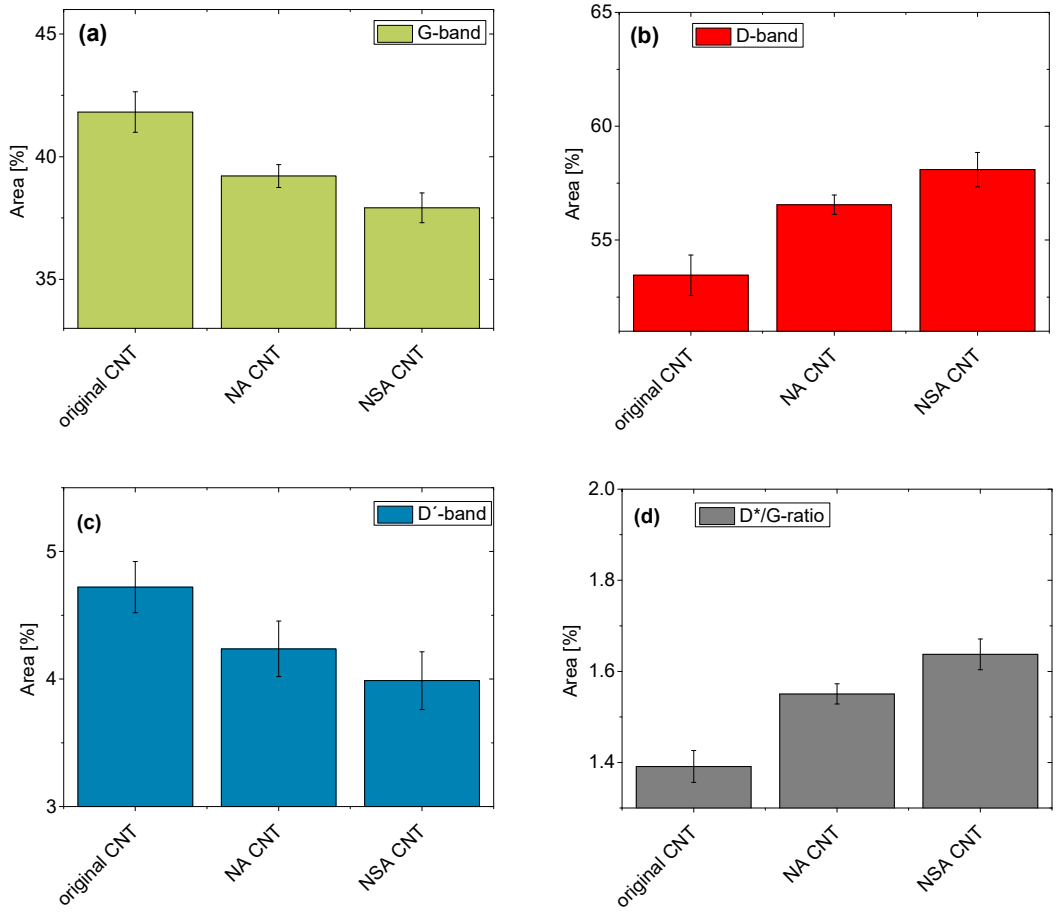

Figure S4. Raman deconvolution results of different samples. The deconvolution was done by a three peaks method, which has been published by our group (*Materials Science and applications*, **2017**, 8, 628-641). Raman spectra of different samples were obtained upon excitation at 532 nm.

Based on our previous work (Carbon 2018, 130, 614) oxygen functional groups can be selectively removed at different temperature: carboxylic group (252 °C), lactone group on zig-zag edge (310 °C), anhydride group (515 °C), lactone group on armchair edge (610°C), phenol group (800 °C) and carbonyl group (1000 °C). Figure S5 shows the detailed information of the functional groups and the related thermal stability.

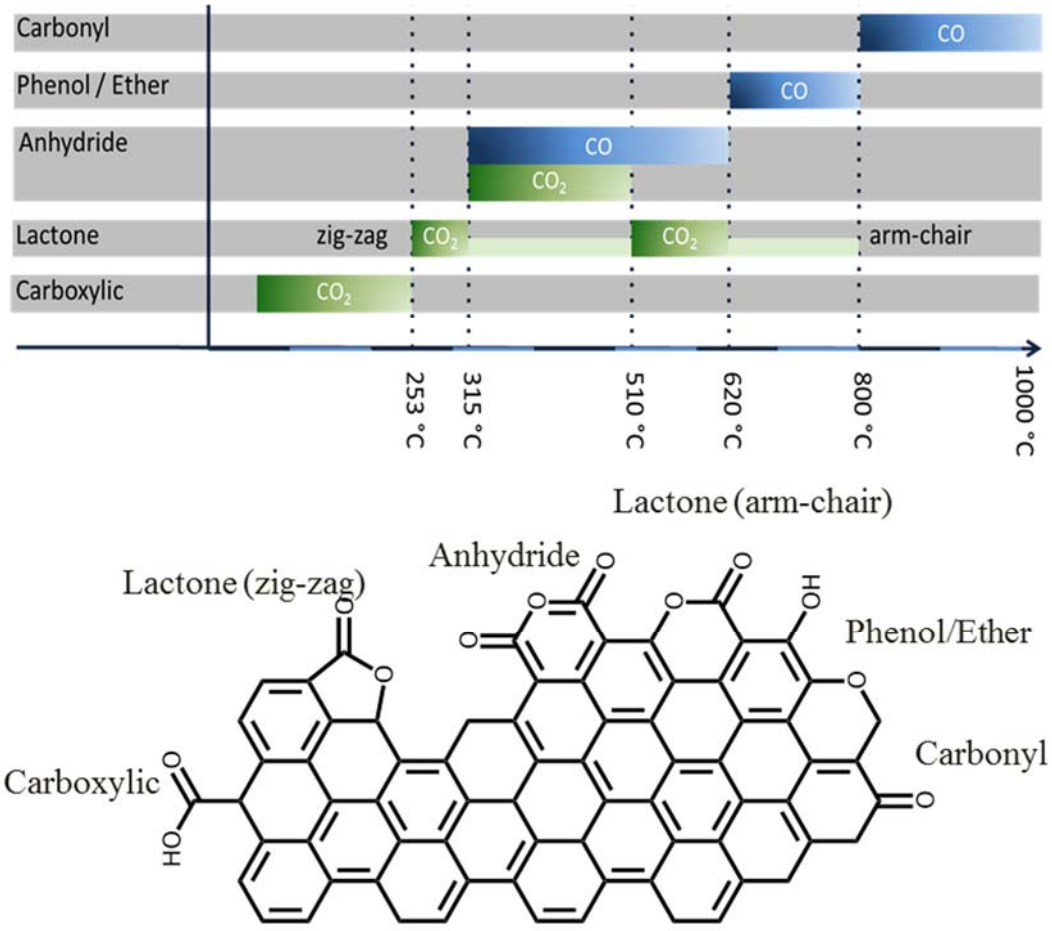

Figure S5. Schematic illustration of the carbon surface oxygen functional groups and the related decomposition temperatures. CO_2 and CO are the decomposition products of the functional groups.

Figure S6 and Figure S7 give the direct evidence of the different functional groups from the non-linear annealing procedure of different CNT samples. The signal of CO^+ and CO_2^+ is normalized to per mg samples. Therefore, the comparison of the peak area in Figure S6 and S7 gives the direct quantitative comparison of the samples. It can be seen that for the original CNT, the amount of the oxygen functional groups is almost negligible. After the treatment with nitric acid, NA CNT gets some functional groups on the surface, while compare with the NSA CNT, the amount of the functional groups is still not high. This means that the functionalization process with mixed acid can introduce a lot of defects and functional groups together.

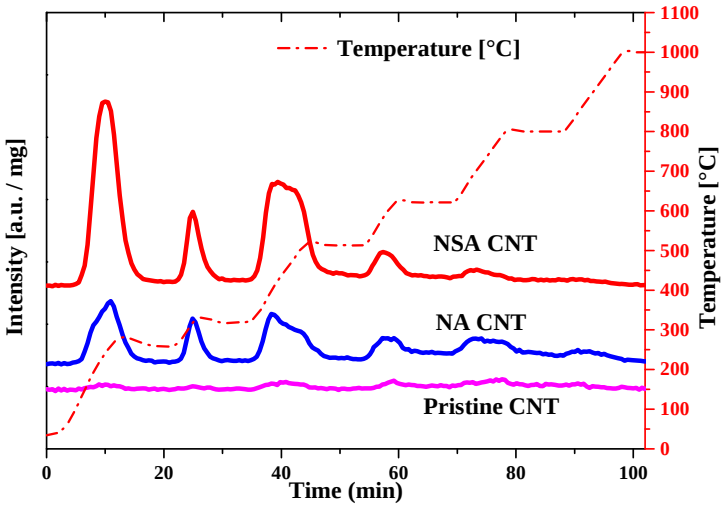

Figure S6. TPD results of the NSA CNT, NA CNT and pristine, respectively. Ion currents of CO_2^+, which is obtained from m/z signal of 44. Red dashed line visualizes the temperature profiles during the experiment.

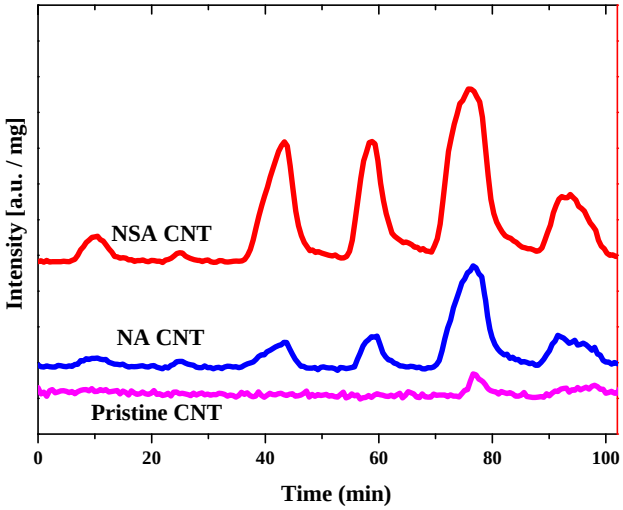

Figure S7. TPD results of the NSA CNT, NA CNT and pristine, respectively. Ion currents of CO^+, which is obtained from m/z signal of 28. The TPD results share the same temperature program as in Figure S6.

Oxygen functional groups on carbon surface have a broad oxidative peak in the cyclic voltammogram at around 0.5 V (Figure S8). This confirms that carbon especially functionalized carbon is easily being oxidized at even very low potential. This cyclic voltammogram curves also suggest the functional groups in this potential range have redox process. The high-temperature annealing in argon condition can remove the oxygen functional groups as well as the capacitance in the CV measurement. Actually, the removal of oxygen functional groups on carbon surface also leads to a relative hydrophobic surface, which increases the contact barriers between the electrolyte and carbon surface. From this point, we can also see the importance of the oxygen functional groups of the carbon material for the electrochemistry behavior.

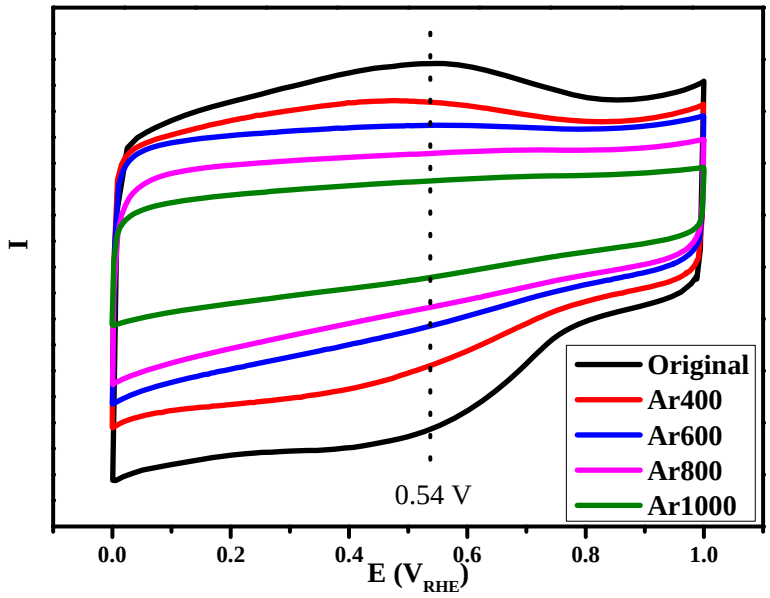

Figure S8. CV of different CNTs annealed at different temperatures (400, 600, 800 and 1000 ^{o}C) under argon condition. CV is conducted from 0 V_{RHE} to 1.0 V_{RHE} at 100 mV/s.

Carbon defects are still not well defined due to their complexity. From the best of our understanding, dangling bonds, non-six-membered rings, functional groups, heteroatoms dopants in the graphitic lattice and C-H bonds in the edge or middle of a perfect graphitic domain are the main forms of the carbon defects. In general, dangling bonds are highly active thus easily being saturated by forming oxygen functional groups, while C-H bonds and non-six-membered rings is relative inert comparing to the functional groups and dopants. Therefore, in the chosen graphitic CNT, oxygen functional groups contribute the main defects for the carbon structure.

In Figure S9, we show the functional groups evolution process in the electrolyte. As carbon surface is very complicated, only several typical functional groups models are list here. Yet, after hydrolysis, COO-, C-O^- and C=O groups become dominated groups on the carbon surface, while with the potential exertion, the C=O can transform into C-O^-.

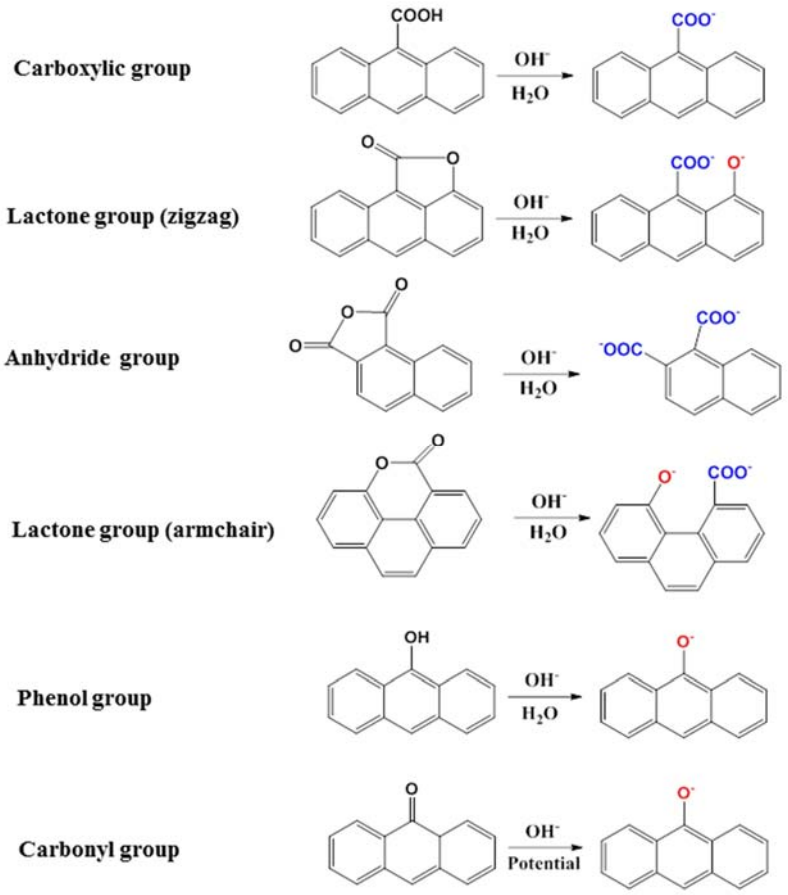

Figure S9. The evolution of the different functional groups on carbon surface during the electrochemical process in the alkaline electrolyte is given in the scheme. The blue color indicates the inactive ones, while the red color indicates the one contribute to the final activity.

In general, the desorption of phenol and carbonyl groups are detected as CO^+ signal like in Figure S6. However, when the CNT samples are mixed with the electrolyte, the desorption of the related functional groups then transfers into CO_2^+ signal as shown in Figure S11, while no obvious peaks for CO^+ signal can be observed (Figure S10). This can be traced back to the formation of C-O-Fe species on the carbon surface, which will be discussed in the following part (Figure S25). The small shift of the phenol group to carbonyl group during the reaction can be observed directly from the peak areas of the CA-20 min sample and the CA-2 h sample. Yet the total content of the functional group has no obvious change. This evidences that during the reaction the phenol group and carbonyl group can be transformed with each other. Although lactone and anhydride groups also exist, which most likely result from the secondary oxidation, their amount are very low as compared to the other three main groups (carboxylic, phenol and carbonyl groups). In addition, those peaks are also influenced by the noise from the measurement, so we do not consider these functional groups here.

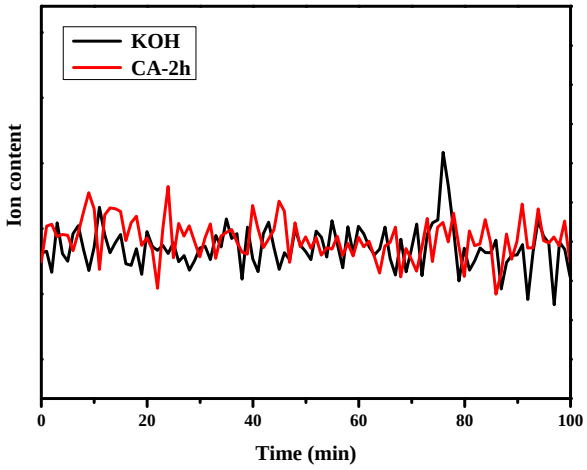

Figure S10. TPD result of the NSA CNT soaked by KOH and after 2 h CA test. Ion currents of CO^+ are used here.

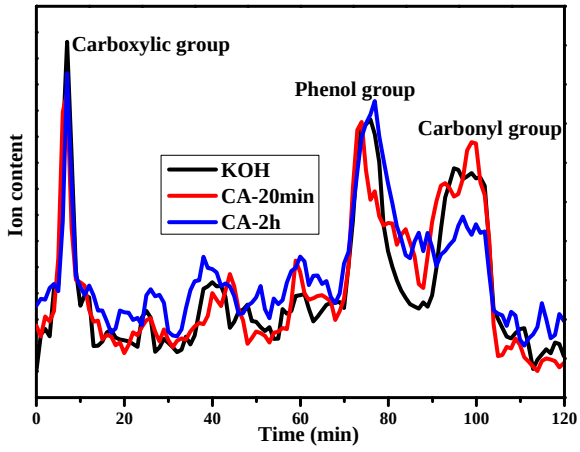

Figure S11. TPD result of the NSA CNT soaked by KOH, after 20 min and 2 h CA test. Ion currents of CO_2^+ are used here.

Carbon is easier to be oxidized than water. With carbon oxidation, a fresh surface will be exposed and new functional groups should be continuously consumed and then formed. If the functional groups are continuously consumed and then in-situ formed, the oxygen in water molecules should also be involved for forming the new oxygen functional groups in the carbon structure. However, when ^{18}O-labeled water is used, even after two-hour CA reaction, no ^{18}O-containing carbon oxides are formed from the decomposition of the reacted CNTs (Figure S12). This means that the oxygen functional groups on the NSA CNT surface maintain the same before and after reaction. And there must be some newly formed species covered the functional groups and protect them from deep oxidation. Figure S21 also gives direct evidence that the CNT is not being oxidized during the reaction, suggesting a good stability for the anode material. Actually, highly graphitic structure is hydrophobic and not easy being oxidized, that's why people always argue that carbon is chemical inertness. The part can be oxidized is generally from edge and vacant part, which have already been oxidized in the functionalization process and terminated by C-H or oxygen functional groups. That's why there is no obvious oxidation process happened on carbon even at high potential.

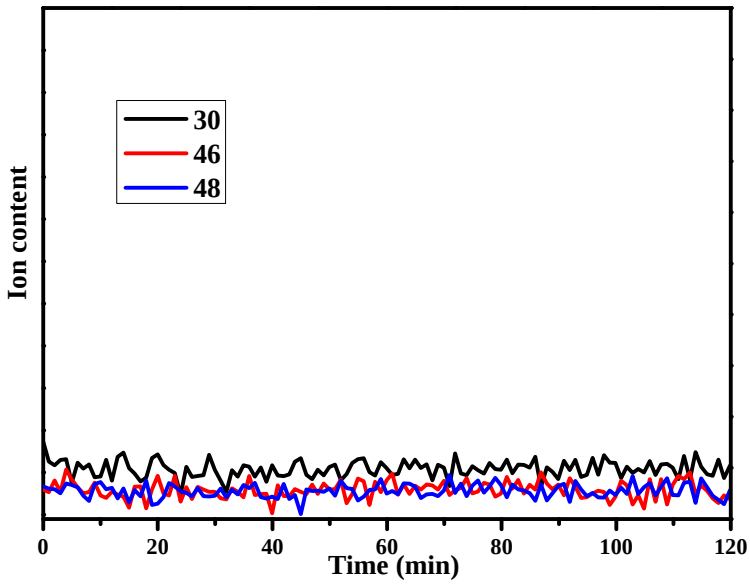

Figure S12. TPD result of the NSA CNT after 2 h CA test in labeled $H_2{}^{18}O$ diluted electrolyte. The content of the labeled water in the electrolyte is 50%. Ion currents of $C^{18}O_2{}^+$ (m/z 48) $C^{16}O^{18}O^+$ (m/z 46) and $C^{18}O^+$ (m/z 30) were shown here. No peaks can be observed for these labeled oxides.

Figure S13 gives the CA test of the 1000°C annealed sample. At this temperature, all carboxylic group, phenol group and carbonyl groups are removed, indicating an almost oxygen-free surface. Yet the removal of the functional groups brings the unstable dangle bonds on the carbon surface, making it vulnerable to the hydroxide in the alkaline electrolyte. During the reaction, some vacant positions resulted from the desorption of oxygen functional groups could be directly oxidized to form phenol groups, while part of them are more stable and need the oxidation potential helping the formation of the phenol groups. This is why from the beginning, it shows around 5 mA/cm^2 current density and finally reaches to around 8 mA/cm^2 at three hours.

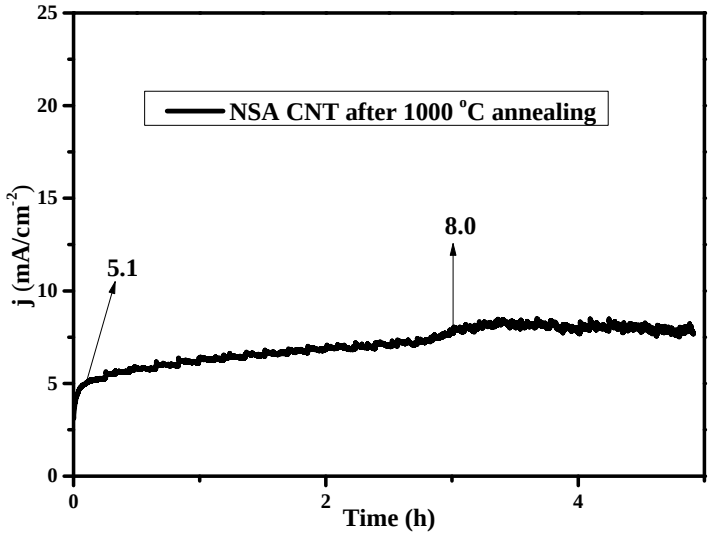

Figure S13. Stability of NSA CNT (annealed at 1000 °C). The potential is kept at 1.8 V.

In general, 1000ºC can remove all the oxygen functional groups mentioned above. Yet when we check the TPD of the samples after soaked into electrolyte and after reaction, a newly raised phenol peak can be observed. With the conduction of the reaction, some carbonyl groups also form. Not like the case in Figure 1c, in which carbonyl group transfer into phenol groups; in the annealed sample, phenol group as dominated functional groups before reaction will transform into carbonyl groups. This also evidences the phenol and carbonyl groups transform with each other during the reaction.

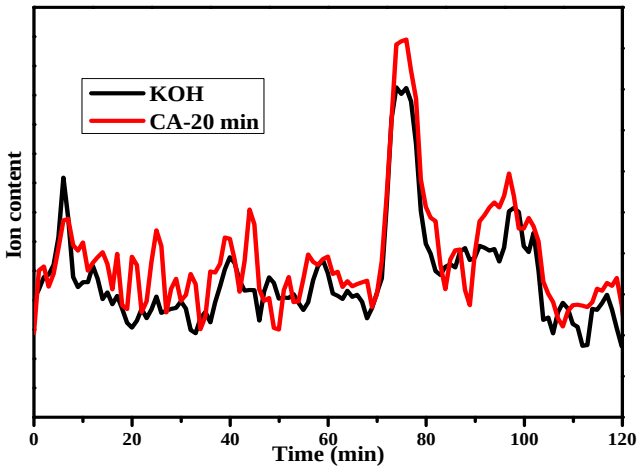

Figure S14. TPD results of the NSA CNT soaked by KOH, after 20 min. Ion currents of CO_2^+ are used here.

In a typical procedure, 50 mg (up) or 25 mg (down) NSA CNT are added into 30 ml 0.1 M KOH; the solution is shook sufficiently to get a good dispersion; then the mixture is placed on a table waiting for a gravity separation of the CNT and the solution (1 hour). Then we use a burette to dip 18 ml supernatant into the small glass bottle with the additional 18 ml fresh KOH, and repeat the same procedure. From the images we can see that by repeatedly washing the CNT, the supernatant becomes more and more transparent. While the one containing more CNT (50 mg, up) show much darker color as compared to the one with less content of CNT. This means that by using these washing processes, the unstable amorphous part can be removed from the CNT surface making the solution brownish. With the removal of the amorphous part, the supernatant become transparent and the following washing process cannot remove the highly graphitic part of the CNT.

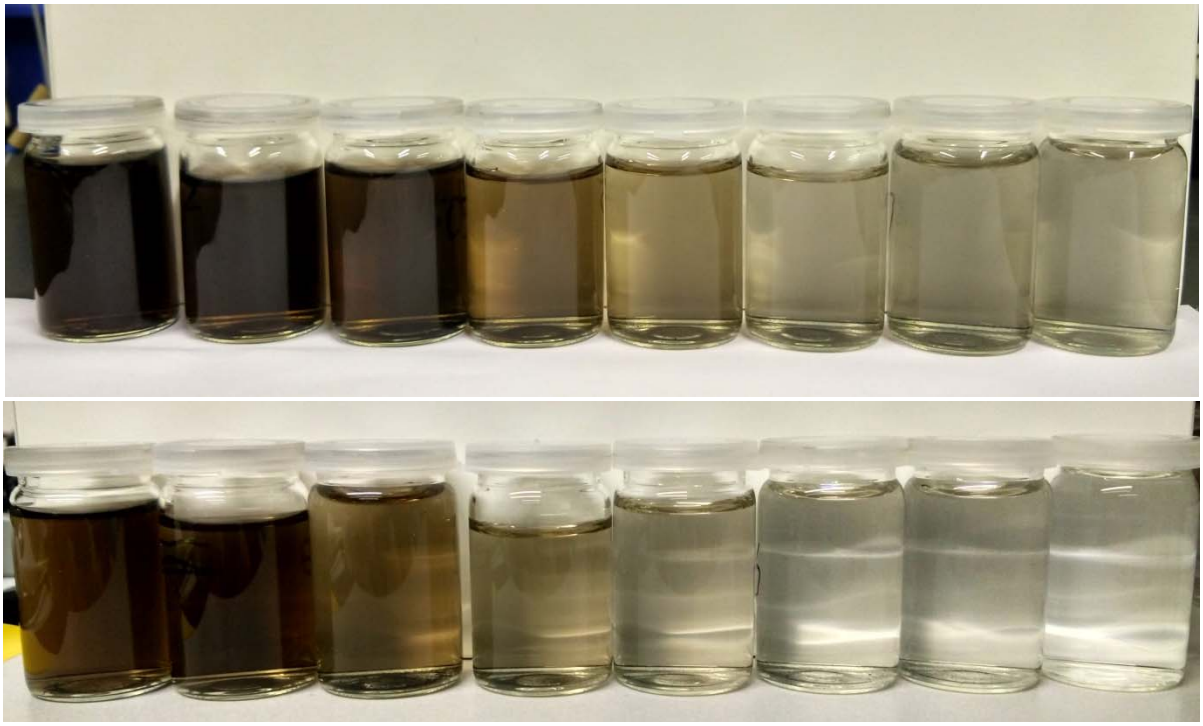

Figure S15. Photo images of the supernatant of the KOH solution after soaking the NSA CNT for 20 min.

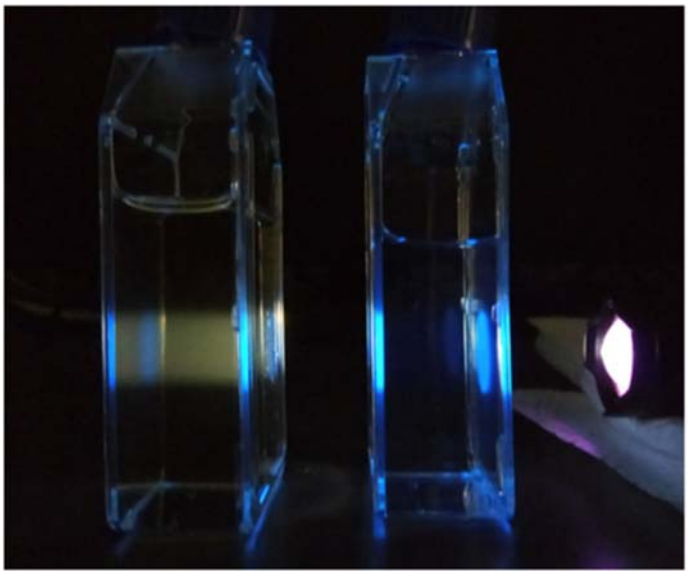

Figure S16. Photo image of electrolyte (right) and the liquid supernatant (left) of electrolyte after soaking the NSA CNT for 20 min and being exposed to ultraviolet light.

Ultraviolet–visible (UV) spectroscopy of the brownish electrolyte after just soaking process is shown in Figure S17. The measurement of the original 0.1 M KOH electrolyte was subtracted as baseline. It shows a broad adsorption and some shoulder peaks as the arrows pointed in the UV spectrum, which means the dissolved part is very complicated (including benzene ring adsorption in the graphitic structure). From high-performance liquid chromatography, we did not get any peaks. This also suggests there might be no small organic species in the brownish electrolyte. Therefore, the dissolved part contains only some carbon quantum dot. Both the UV spectrum and quantum effects indicate only small pieces of amorphous part are removed and the graphitic backbone is stable in the electrolyte.

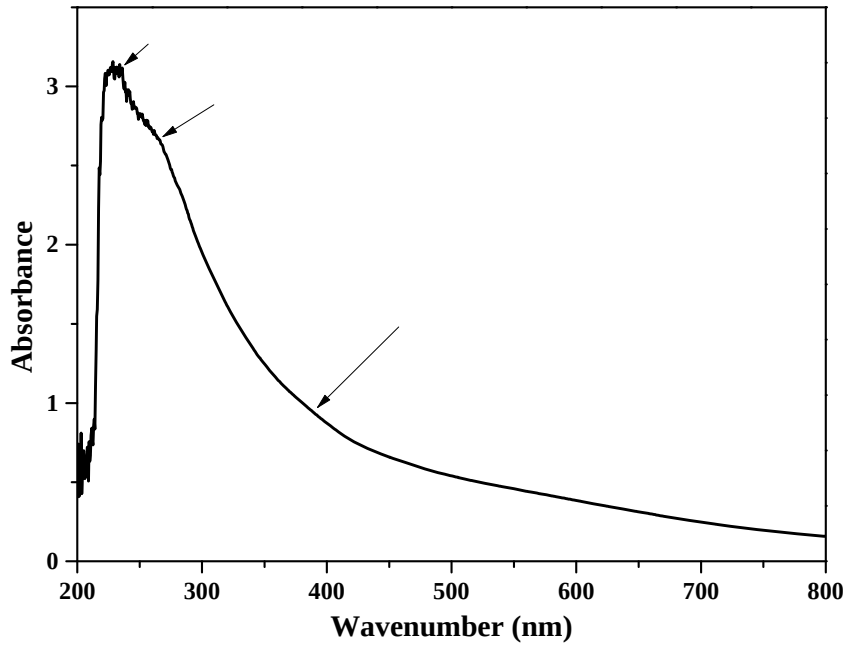

Figure S17. Ultraviolet–visible (UV) spectroscopy of the brownish electrolyte after just soaking process.

In Figure S18, both washed and unwashed CNT show similar electrochemical redox peaks from the potential range from 0 V to 1.0 V. Compared to the same behavior of the non-oxygen contained sample in Figure S10, which shows the disappear of the redox peak, the washed process apparently has no influence on the oxygen functional groups. The removal of the amorphous carbon is different from the removal of the functional groups. In other words, amorphous part on the CNT surface is mostly physical adsorbed. Therefore, the electron transfer is limited. This also explains that in Figure S19, the electrochemical behaviors of the washed and unwashed CNT are similar.

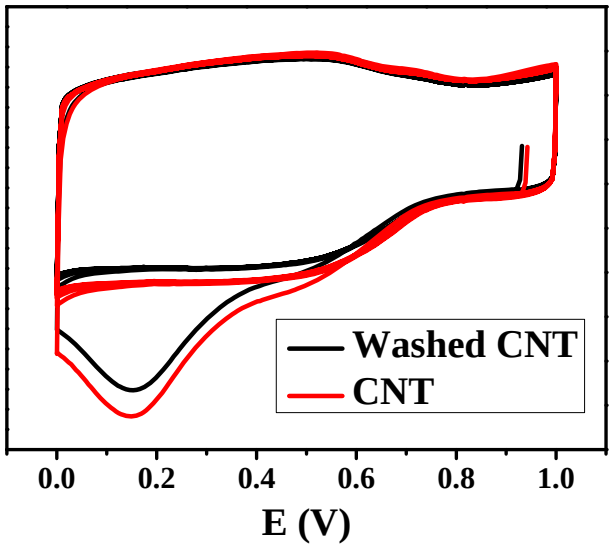

Figure S18. CV of CNTs and the washed CNTs. CNT is the original NSA CNT and the washed CNT is the same batch but without amorphous carbon on the surface.

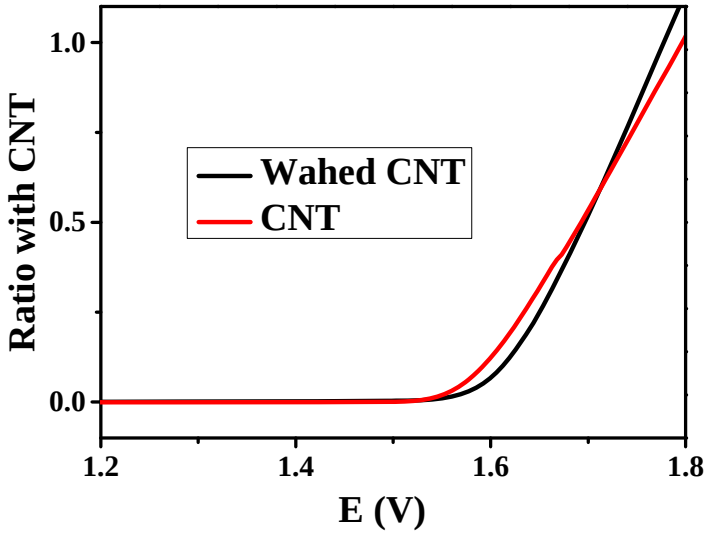

Figure S19. Normalized activities of the original CNT and the washed one.

Figure S20 shows the TEM images of the NSA CNT before and after reaction. The CNT before reaction has a lot of amorphous carbon on the surface and the organic-like amorphous part also causes the blur image from the TEM measurement. In contrast, the CNT after reaction exhibits a clean surface without the attachment of the amorphous part. Accordingly, the removal of the amorphous part introduces a clear image for the sample.

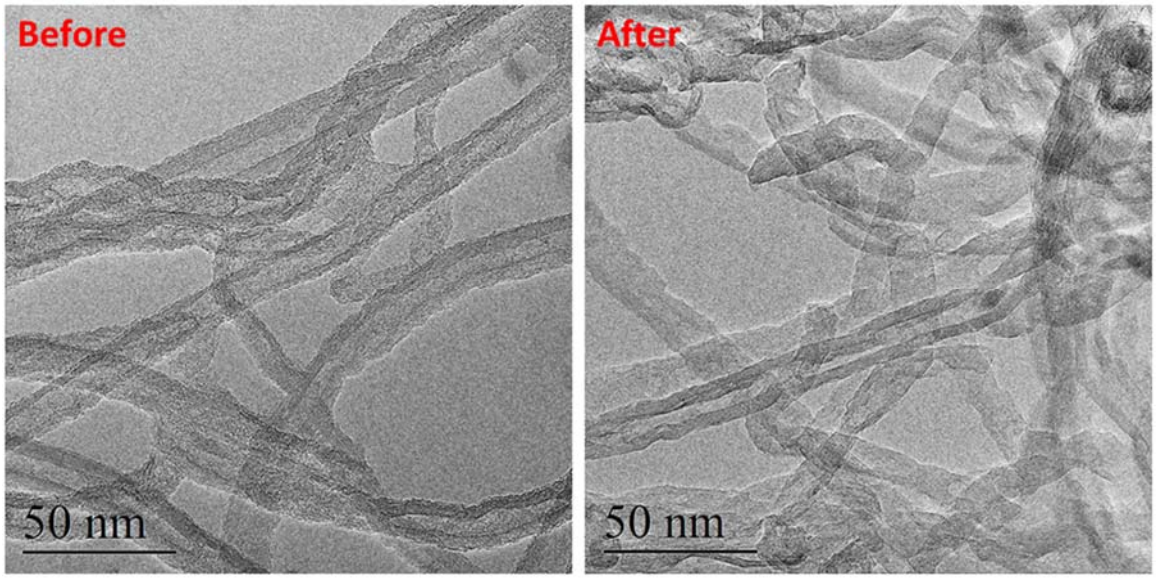

Figure S20. TEM images of the NSA CNT before and after 2 hours CA tests.

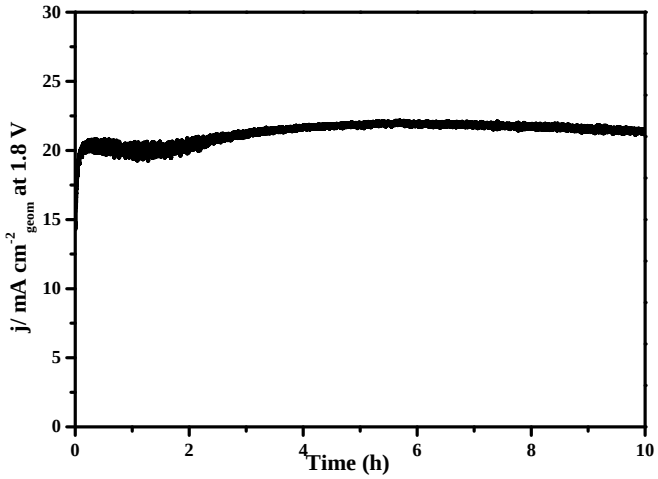

Figure S21. Stability of NSA CNT (annealed at 400 ºC). The potential is kept at 1.8 V_{RHE} for 10 hours.

Figure S22 shows the CA test of the NSA CNT in untreated electrolyte (4 ppb iron) and treated electrolyte (close to 0 ppb iron). Without the iron species cover the functional groups and protect it from deep oxidation, the low current in the purified electrolyte cannot last. The decease of the current might be caused by the oxidation and removal of carbon functional groups from carbon surface.

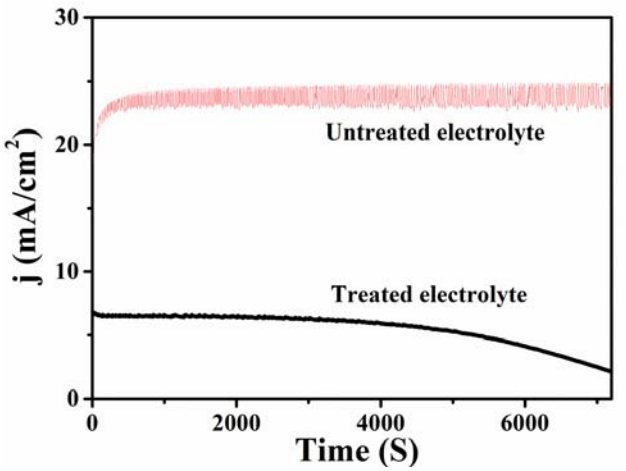

Figure S22. Stability of NSA CNT in purified and unpurified electrolyte. The potential is kept at 1.8 VRHE for 2 hours.

As phenol group in alkaline media exists as $–O^-$, the adsorption energy of phenol group with the ionic Fe^{3+} is confirmed as -38.4 eV (Figure S23), which is highly active. Considering the low concentration of the iron impurity in the electrolyte, the full engagement of the phenol group cannot be promised even though the adsorption propensity is high. The calculated Mayer bond order 0.7 suggests that a weak chemical bond could be formed upon the interaction of Fe^{3+} with the functional group. This endows the electron transfer between the iron site and the carbon anode. When the Mayer bond order is lower than 0.5, no chemical bond can form between the species; when the Mayer bond order is higher than 0.5 and lower than 1, weak chemical bond could be formed; when the Mayer bond order is higher than 1, strong chemical bond can be formed between the species.

Figure S23. The adsorption energy of hydroxyl and Fe species. As the iron species is in alkaline and oxidation media, Fe^{3+} is considered as main species. The structure is represented by a molecular model, which is optimized at the B3LYP/6-31+G* level, and the energy is further refined at the B3LYP/6-311++G** level of theory. All calculations are performed by using the Gaussian 09 program.

As compared to the phenol group ($–O^-$), carbonyl group shows much lower adsorption energy of -24.9 eV (Figure S24). However, it is strong enough for a quick adsorption. In order to form a chemical bond with the iron cation, the -C=O will transfer into a single bond. This transformation could also happen before the adsorption process. In the electrolyte, the phenol groups and carbonyl groups could transform into each other with a very low energy of 0.2 eV as shown in Figure S24. Obviously, O^- from phenol group is more favorable to form a chemical bond with the iron ion, as the Mayer bond order for the C-O-Fe formed with carbonyl group is lower than that of with the phenol group. This might cause the shift of the equilibrium to the phenol side. Nevertheless, it is safe to say that both phenol and carbonyl groups contribute to the formation of the catalytically active site; the bond between carbon atom and oxygen is a single bond and the bond between iron and oxygen should also be a single bond, which means the –C-O-Fe species can be confirmed.

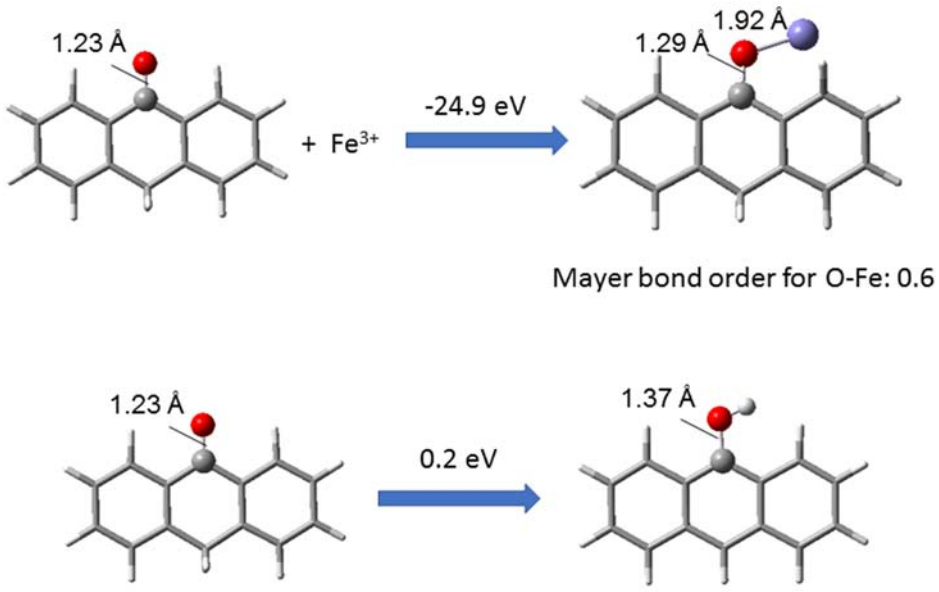

Figure S24. The adsorption energy of carbonyl group and Fe species (up) and the transformation from carbonyl group to phenol group (down). The structure optimization is carried out at the B3LYP/6-31+G* level, and the energy is further refined at the B3LYP/6-311++G** level of theory. All calculations are performed by using the Gaussian 09 program.

In Figure S25, the bump (the arrow part) of the Fe 2p peak also somehow supports the presence of the iron after the reaction. However, similar with the NEAXFS, the iron peak in the XPS spectrum is too small to analyze the exact species of the iron, since the iron content on the carbon surface is rather low. It is easy to understand that in the electrolyte, the iron content is four ppb, which is hard to detect already. When it is partly adsorbed on the carbon surface, to the best of our knowledge, there is no technique currently which is capable to tell what the exact species has been formed.

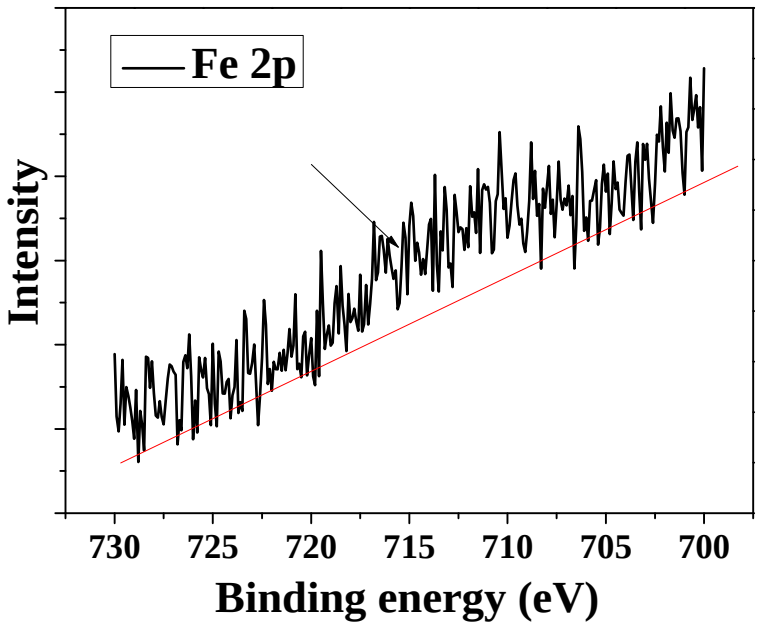

Figure S25. Fe 2p XPS spectrum of the CNT sample after CA test.

As indicated in Figure S23, C-O-Fe$(OH)_x$ species is most likely formed. Considering the oxidation as well as the alkaline environment, the iron ions should be Fe^{3+}. Therefore, we propose the iron active sites on carbon as C-O-Fe$(OH)_2$ (Figure S26). This can be supported by the TPD experiments. As mentioned above, TPD signal for the desorption of phenol group is generally CO^+. However, in the electrochemical treated samples, we get only 44 signal, which is attributed to CO_2^+. The formation of the C-O-Fe$(OH)_2$ could explain this behavior. As shown in Figure S26, the heating procedure will firstly break the iron hydroxide C-O-Fe$(OH)_2$ at very low temperature to form a water and C-O-Fe=O. The anchoring process of the iron does not change the stability of the part in the red box. Therefore, it decomposes at the same temperature as the original phenol group did to form CO. The CO is reductive gas, and it is easy to reduce the Fe=O to form metallic iron and CO_2^+, especially at such high temperature of TPD. Therefore, the change of CO^+ signal to CO_2^+ signal in TPD is a very convincing evidence for the proposed iron structure. The dynamic process mentioned in Figure S9, can also support the formation of the C-O-Fe species.

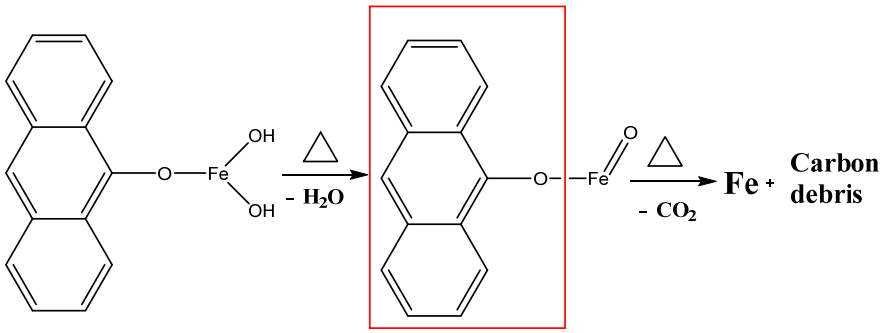

Figure S26. Proposed active iron species on the carbon surface.

The ICP-OES measurement was in-situ conducted in a flow cell with 1 M KOH (iron content is 40 ppb) as the detect limitation of the equipment is not able to detect the change when the iron content is very low. A coil-shaped platinized platinum wire (PT-5W, 125µm diameter, 99.99%, Science Products GmbH), placed along the flow channel following the electrolyte flow, was used as the counter electrode (CE), while the reference electrodes (RE) (Hg/HgO, CH Instruments Inc., CHI152, reference potential +0,098Vvs NHE) was inserted perpendicular to the electrolyte outlet channel. Catalysts were drop casted on glassy carbon support measuring a surface area of 0.196cm^2, previously polished with fine 0.05µm and 1.0µm alumina powder and ultra-sonicated for 15min in MilliQ water. Catalyst inks were prepared by mixing by ultra-sonication 49% H_2O, 49% ethanol and 2% Nafion solution for 30min. Subsequently a certain amount of catalyst ink was drop casted on the glassy carbon working electrode (WE) until a loading of 100 µg/cm^2 was achieved. The catalyst ink was dried on the glassy carbon support under an Argon stream for 30min and finally the working electrode sample holder was inserted into the flow cell. A flow rate of 0.86ml/min was used, because it provides a good balance between oxygen gas removal from the catalyst surface and sufficient detection of the catalyst corrosion products in the ICP-OES. Lower flow rates prohibit reproducible experimental conditions due to excessive oxygen bubble formation at such high current densities. Transient signals of iron were recorded continuously with an integration interval of 100ms and 2 sweeps per reading. The ICP result shows a slight decrease of the iron content in the electrolyte while CNT is used as the electrode material, which confirms the in-situ reaction between the CNT surface and the iron impurity in the electrolyte. When the reaction stopped, the iron content out the electrolyte increased again.

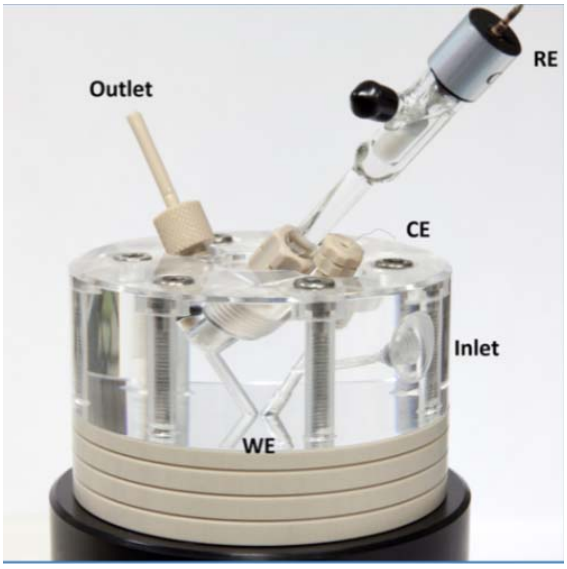

Figure S27. Flow cell setup for in-situ ICP-OES measurement.

FeSSIL/Graphene and FeSSIL/CNT were synthesized according to the reported method (Angew. Chem. Int. Ed. 2018, 57, 3514 –3518), in which we substitute the Co precursor with iron precursor. The final iron content of the both sample supported on CNT and graphene are 5wt%. The FeNC is synthesized by mixing 200mg CNT, 70mg $Fe(CH_3COO)_2$ and 300 mg 1-Ethyl-3-methylimidazolium dicyanamide and annealing at 900°C for 2h under argon condition. The final iron content is around 8wt%. From Figure S28, although these samples have more iron content than the system in the current case, they show much lower activity. Besides, these samples all suffer serious deactivation problem. Especially for the graphene supported sample, the carbon oxidation process can even be observed in Figure S28. That means iron in the structure of C-O-Fe system is good catalyst with good stability. The dynamic formation process might be favorable for the good stability. Other iron species show worse activity, which also evidence that the structure of the iron species is quite important for the final performance. This also explained why compared to other metals, iron always show worse activity. The current system is useful for fabricating efficient water splitting devices. In the following work, different metals will be checked and we think the Fe might be replaced by some metals. However, the mechanism with other metals could be totally different with iron species. We have checked the Ni^{2+}. When we add 4 ppb of Ni^{2+} in the electrolyte, the activity of the CNT has almost no change. Only after oxidation process at higher potential, the activity show a little increase, but still much lower than the iron case. The stability is also not good. This may need better ratio of metal species to improve. We need more work to explain this, as each metal behavior may be totally different.

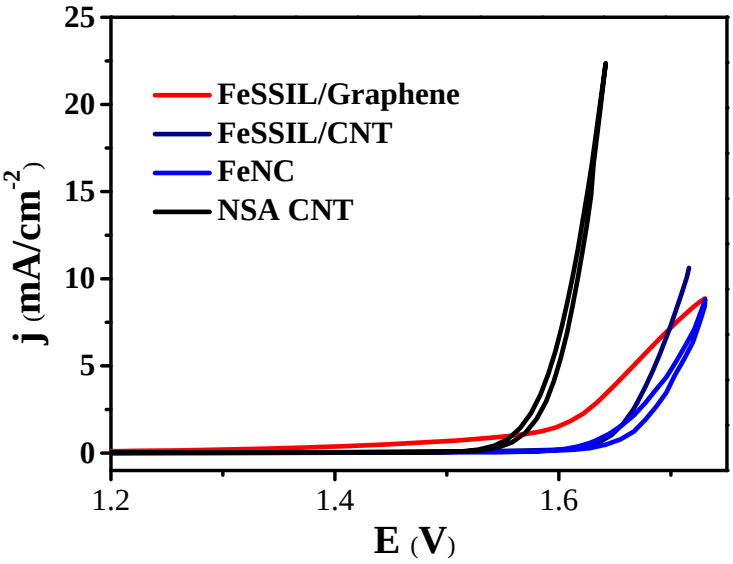

Figure S28. Different iron-based catalyst for the comparison with the C-O-Fe system at the same conditions.

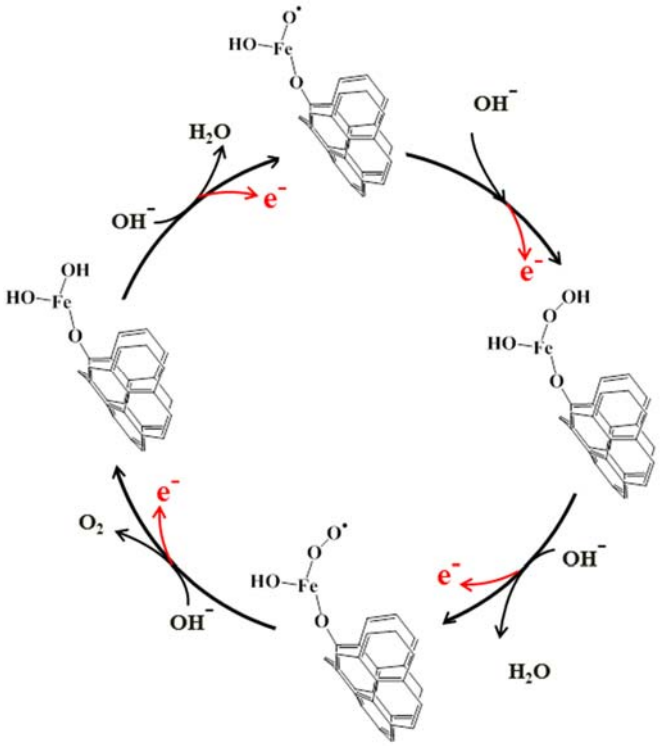

Figure S29. Proposed mechanism. Possible evolution steps of the adsorbed iron species on CNTs during the oxygen formation process.

Detailed experimental information and discussion of Figure 4

Figure 4a shows how the systematically varied iron contents in the electrolyte influence on the reaction. When the iron content is lower than four ppb, the current at 1.8 V increase with the increase of the iron contents. The un-overlapped curves with low iron contents give the most direct evidence for the dynamic formation of the intrinsically active sites. It means that the lower iron content in the electrolyte, the longer time it takes to reach a stable equilibrium of the dynamic anode system, which is caused by the limitation of the mass transport when the iron content in the vicinity of CNT is very low. While we keep increasing the iron content in the electrolyte after four ppb, the activity is decreased a little. This might be caused by the degradation of the extra iron with hydroxide or the agglomeration of the iron species on the CNT surface.

Every time we start a new reaction, it needs an initial step to reach a stable current. Therefore, we conducted a programmed CA test with 1.8 V→ 0V→1.8V→0V→… procedure, from which an around eight-minute initial step is always needed (Figure 4b). This means that some of the "active sites" might dynamically form at high potential, while at low potential the dynamic

process does not happen. The initial step could be a saturation process for the dynamic formation of the active sites. The slightly decrease of the current for the sequential turns most likely comes from the detachment of the sample from the electrode surface. From the theoretical calculation in Figure S23, the calculated Mayer bond order of 0.7 suggests a weak bond formed between the iron species and the functional groups. Actually, this also can explain why the active sites are dynamically formed. When the high potential is applied, carbon surface become more attractive to the iron species and form relative stable C-O-Fe species; when the potential is removed, the interaction between iron species and carbon surface become not strong enough to form a stable chemical bond, thus lead to the removal of iron species from the carbon surface. Therefore, in the mechanism in Figure S29, the bond between iron and C-O- is only detectable at high potential. Physical adsorption of iron could also happen, but only with a very small amount.

A pulsed technique is used to confirm the presence of iron (Figure 4c). DPV measurements show that with standard electrolyte (4 ppb iron), the NSA CNT show an iron oxidation peak at around 0.5 V. The iron might come from the non-selective adsorption of the iron on CNT surface; while after the CA test at 1.8 V, a much higher oxidation peak can be observed. This means more iron species are formed during the OER process. After a CV test from 1 V_{RHE} to 1.8 V_{RHE}, where the potential stopped at 1 V, the iron content recovers to the initial level, which indicates that the in-situ formed iron species are not stable and can easily decompose.